

THE ROLE OF FIXED DELAYS IN NEURONAL RATE MODELS

ALEX ROXIN AND ERNEST MONTBRIÓ

ABSTRACT. Fixed delays in neuronal interactions arise through synaptic and dendritic processing. Previous work has shown that such delays, which play an important role in shaping the dynamics of networks of large numbers of spiking neurons with continuous synaptic kinetics, can be taken into account with a rate model through the addition of an explicit, fixed delay. Here we extend this work to account for arbitrary symmetric patterns of synaptic connectivity and generic nonlinear transfer functions. Specifically, we conduct a weakly nonlinear analysis of the dynamical states arising via primary instabilities of the stationary uniform state. In this way we determine analytically how the nature and stability of these states depend on the choice of transfer function and connectivity. While this dependence is, in general, nontrivial, we make use of the smallness of the ratio in the delay in neuronal interactions to the effective time constant of integration to arrive at two general observations of physiological relevance. These are: 1 - fast oscillations are always supercritical for realistic transfer functions. 2 - Traveling waves are preferred over standing waves given plausible patterns of local connectivity.

1. INTRODUCTION

When studying the collective dynamics of cortical neurons computationally, networks of large numbers of spiking neurons have naturally been the benchmark model. Network models incorporate the most fundamental physiological properties of neurons: sub-threshold voltage dynamics, spiking (via spike generation dynamics or a fixed threshold), and discontinuous synaptic interactions. For this reason, networks of spiking neurons are considered to be biologically realistic. However, with few exceptions, e.g. [Amit and Brunel(1997)], [Brunel and Hakim(1999)], [Brunel(2000)], network models of spiking neurons are not amenable to analytical work and thus constitute above all a computational tool. Rather, researchers use reduced or simplified models which describe some measure of the mean activity in a population of cells, oftentimes taken as the firing rate. Firing-rate models are simple, phenomenological models of neuronal activity, generally in the form of continuous, first-order ordinary differential equations [Wilson and Cowan(1972)]. Such firing-rate models can be analyzed using standard techniques for differential equations, allowing one to understand the qualitative dependence of the dynamics on parameters. Nonetheless, firing-rate

Date: October 5, 2009.

models do not represent, in general, proper mathematical reductions of the original network dynamics but rather are heuristic, but see [Ermentrout(1994)]. As such, there is in general no clear relationship between the parameters in the rate model and those in the full network of spiking neurons, although for at least some specific cases quasi-analytical approaches may be of value [Shriki et al.(2003)]. It therefore behooves the researcher to study rate models in conjunction with network simulations in order to ensure there is good qualitative agreement between the two.

Luckily, rate models have proven remarkably accurate in capturing the main types of qualitative dynamical states seen in networks of large numbers of asynchronously spiking neurons. For example, it was shown in [Roxin et al.(2005)], [Roxin et al.(2006)] that the addition of an explicit delay in a rate equation was sufficient to describe the emergence of fast oscillations prevalent in networks of spiking neurons with dominant inhibition. In such networks, effective delays due to the continuous synaptic kinetics can lead to oscillations even in the absence of any explicit delay in the neuronal interactions. When the pattern of synaptic connectivity depends on the distance between neurons, then this effective delay can also lead to the emergence of waves. This is certainly a relevant case for local circuits in cortical tissue, where the likelihood of finding a connection between any two neurons decreases as a function of the distance between them, e.g. [Holmgren et al.(2003)]. In [Roxin et al.(2005)], [Roxin et al.(2006)], the authors studied a rate model with fixed delay on a ring geometry with two simplifying assumptions. First they assumed that the strength of connection between neurons could be expressed as a constant plus the cosine of the distance between the neurons. Secondly, they assumed a linear rectified form for the transfer function which relates inputs to outputs. These assumptions allowed them to construct a detailed phase diagram of dynamical states, to a large degree analytically. In addition to the stationary bump state (SB) which had been studied previously [Ben-Yishai et al.(1995)], [Hansel and Sompolinsky(1998)], the presence of a delay led to two new states arising from primary instabilities of the stationary uniform state (SU): an oscillatory uniform state (OU) and a traveling wave state (TW). Secondary bifurcations of these three states (SB,OU,TW) led to yet more complex states including standing waves (SW) and oscillatory bump states (OB). Several regions of bistability between primary and secondary states were found, including OU-TW, OU-SB and OU-OB. They subsequently confirmed these results through simulations of networks of Hodgkin-Huxley neurons. Despite the good agreement between the rate equation and network simulations, two main issues remain unresolved.

- The rate equation predicted that the primary instability of the SU state to waves should be to traveling waves, while in the network simulations standing waves were robustly observed.

- The linear-threshold transfer function, albeit amenable to analysis, nonetheless leads to degenerate behavior at a bifurcation point. Specifically, any perturbations with a positive linear growth rate will continue to grow until the lower threshold of the transfer function is reached. This means that the amplitude of new solution branches at a bifurcation is always finite, although the solution itself may not be subcritical. In a practical sense then, this means that it is not possible to assess whether a particular solution, for example oscillations or bumps, will emerge continuously from the SU state as a parameter is changed, or if it will appear at finite amplitude and therefore be bistable with the SU state over some range.

In order to address these issues, and provide a more complete analysis of the role of fixed delays in neuronal tissue, we here study a rate equation with delay without imposing any restrictions on the form of the transfer function beyond smoothness or on the shape of the connectivity kernel beyond being symmetric. What we show is that the nature and stability of the solutions arising via primary instabilities of the SU state (oscillations, bumps and waves) depend on nonlinear combinations of the first three derivatives of the transfer function and the first three spatial Fourier coefficients of the connectivity kernel. Thus while the presence of a fixed delay alone is sufficient to generate oscillations and waves, whether the oscillations are bistable with the unpatterned state and which type of waves (standing waves or traveling waves), appear as a stable solution, depend crucially on the transfer function and pattern of synaptic connectivity. We will discuss this in great depth in the results section.

We would like to emphasize the fact that we are interested in the effect of a *fixed* delay on the dynamics of a local patch of cortical tissue. In fact, delays in the nervous system are most often associated with transmission delays, i.e. delays due to the finite velocity propagation of action potentials along axons. Indeed, this type of propagation delay, which depends linearly on the distance between any two neurons, has been the topic of much theoretical study, e.g. [Pinto and Ermentrout(2001)], [Coombes et al.(2003)], [Hutt et al.(2003)], [Hutt(2004)], [Atay and Hutt(2005)], [Laing and Coombes(2005)], [Hutt and Atay(2006)], [Venkov et al.(2007)], [Coombes et al.(2007)]. Localized solutions of integro-differential equations describing neuronal activity, including fronts and pulses, are affected by distance-dependent axonal delays [Pinto and Ermentrout(2001)], [Coombes et al.(2003)], [Hutt(2004)], [Hutt and Atay(2006)]. Specifically, the velocity of propagation of the localized solution is proportional to the conduction velocity along the axon for small conduction velocities, while for large conduction velocities it is essentially constant. This reflects the fact that the propagation of activity in neuronal tissue is driven by local integration in which synaptic and membrane time constants provide

the bottleneck. Also, allowing for different conduction velocities for separate excitatory and inhibitory populations can lead to bifurcations of localized bump states to breathers and traveling pulses [Laing and Coombes(2005)]. Pattern-forming instabilities have also been studied in the presence of distance-dependent delays. The presence of propagation delays in rate models can lead to oscillations and waves [Coombes et al.(2003)], [Atay and Hutt(2005)]. The weakly nonlinear dynamics of waves in spatially extended rate models, i.e. describing large-scale (on the order of centimeters) activity, is described by the coupled mean-field Ginzburg-Landau equations [Venkov et al.(2007)], and thus exhibits the phenomenology of small amplitude waves familiar from other pattern forming systems [Cross and Hohenberg(1993)].

On the other hand, fixed delays, and their effect on the dynamics of large numbers of recurrently coupled neurons, have received relatively little theoretical attention. Some exceptions include work on the role of global feedback delay in shaping the power spectrum of a network driven by noisy inputs [Hutt et al.(2008)] and the effect of distributed delays in a mean-field corticothalamic model [Roberts and Robinson(2008)]. More akin to the work we present here is the recent study of the effect of two distinct delays in a spatially homogeneous Wilson-Cowan model [Coombes and Laing(2009)]. There the authors were able to compute oscillatory solutions analytically given a Heaviside transfer function of the rate variables.

More generally, fixed delays, which are likely due to synaptic and dendritic integration, and conduction delays due to the propagation of action potentials along the axon, are both present in real neuronal systems. Importantly, this means that the delay in neuronal interactions at zero distance is not zero. In fact, *fixed* delays are always observed in paired intracellular recordings in cortical slices. The latency from the start of the fast rising phase of the action potential to the start of the post-synaptic current (or potential) has been measured for pairs of pyramidal cells in rat layers 3 to 6 and is on the order of milliseconds, see [Thomson and Lamy(2007)] for a recent review. Recordings from cat cortex and between pyramidal cells and other cells including spiny cells and interneurons in the rat cortex also reveal fixed delays which are rarely less than a millisecond. These delays are seen when neurons are spatially adjacent, indicating that axonal propagation is not an important contributing factor. On the other hand the speed of propagation of action potentials along unmyelinated axons in mammals is on the order of $10^{-1} - 10^1$ m/s, which means a delay of 0.1-10 ms for neurons separated by 1 millimeter [Kandel et al.(1991)], [Girard et al.(2001)]. Thus fixed delays and conduction delays are of similar magnitude within a local patch of cortex and both would be expected to shape the dynamics of non-steady activity, i.e. neither is negligible. Here we have decided to focus on fixed delays, as in previous work [Roxin et al.(2005)], [Roxin et al.(2006)], due both to their physiological relevance and prevalence in networks of spiking neurons.

Thus in what follows we will study a rate equation with fixed delay and spatially modulated connectivity. In section 2 we formulate the model and conduct a linear stability analysis of the SU state. In section 3 we conduct a weakly nonlinear analysis for the four possible primary instabilities of the SU state (asynchronous unpatterned state in a network model), thereby deriving amplitude equations for a steady, Turing (bumps), Hopf (global oscillations), and Turing-Hopf (waves) bifurcations. We will focus on the delay-driven instabilities, i.e. Hopf and Turing-Hopf. Finally, in section 4 we will study the interactions of pairs of solutions: bumps and global oscillations and global oscillations and waves respectively.

2. THE MODEL

We study a heuristic equation describing the activity of a small patch of neural tissue consisting of two populations of recurrently coupled excitatory and inhibitory neurons respectively. Our formulation is equivalent to the Wilson-Cowan equations without refractory period [Wilson and Cowan(1972)], and with spatially dependent synaptic connectivity which was studied originally in [Ermentrout and Cowan(1980)]. Additionally, we consider a fixed delay in the neuronal interactions. Given these assumptions, the full Wilson-Cowan equations are

$$(1) \quad \tau_e \dot{r}_e = -r_e + \Phi_e \left(\int_{\Omega} dy J_{ee}(|x-y|) r_e(y, t-d_e) - \int_{\Omega} dy J_{ei}(|x-y|) r_i(y, t-d_i) + I_e \right),$$

$$(2) \quad \tau_i \dot{r}_i = -r_i + \Phi_i \left(\int_{\Omega} dy J_{ie}(|x-y|) r_e(y, t-d_e) - \int_{\Omega} dy J_{ii}(|x-y|) r_i(y, t-d_i) + I_i \right).$$

In the original formulation [Wilson and Cowan(1972)], $r_e(x, t)$ and $r_i(x, t)$ represent the average number of active cells in the excitatory and inhibitory populations respectively, in this case at a position x and at a time t . The time constant τ_e (τ_i) is roughly the time it takes for a excitatory (inhibitory) cell receiving “at least threshold excitation” [Wilson and Cowan(1972)] to generate a spike. This can reasonably be taken as the membrane time constant which is generally on the order of 10-20 ms. The functions $\Phi_a(x)$ ($a = e, i$) are usually taken to be sigmoidal. Specifically, if all neurons in the population receive equal excitatory drive, and there is heterogeneity in some parameter across neurons, e.g. the threshold to spiking, which obeys a unimodal distribution, then the fraction of active neurons is just the integral over the distribution, up to the given level of excitation. The integral of a unimodal distribution is sigmoidal. In Eqs.1-2, the functions $J_{ab}(|x|)$ ($a = e, i$) ($b = e, i$) represent the strength of synaptic connection from a neuron in population b to a neuron in population a separated by a distance x . Here the neurons are arranged in one dimension on a domain Ω .

Input from excitatory (inhibitory) cells is furthermore delayed by a fixed amount d_e (d_i), which, as we have discussed in the introduction, is on the order of one millisecond. Finally, the excitatory and inhibitory populations are subject to an external drive of strength I_e and I_i respectively.

A general analysis of Eqs.1-2 would be technically arduous although it is a natural extension of the work presented here. Rather, we choose to study the dynamics of this system under the simplifying assumption that the excitatory and inhibitory neurons follow the same dynamics, i.e. $\tau_e = \tau_i = \tau$, $d_e = d_i = d$, $J_{ee} = J_{ie} = J_e$, $J_{ei} = J_{ii} = J_i$, $\Phi_e = \Phi_i = \Phi$, $I_e = I_i = I$. If this the case, then $r_e = r_i = r$ and the variable r follows the dynamics given by

$$(3) \quad \dot{r}(x, t) = -r(x, t) + \Phi\left(\frac{1}{2\pi} \int_{-\pi}^{\pi} dy J(|x - y|)r(y, t - D) + I\right),$$

where we have chosen the domain Ω to be a ring of normalized length $L = 2\pi$. Furthermore, we have re-scaled time by the time constant τ . The normalized delay is therefore $D = d/\tau$, which is the ratio of the effective delay in neuronal interactions to the integration time constant and should be much less than one in general. The synaptic connectivity expressed in terms of the excitatory and inhibitory contributions is $J(|x|) = J_e(|x|) - J_i(|x|)$ and thus represents an effective mixed coupling which may have both positive and negative regions. Eq.3 with the choice of $\Phi(I) = I$ for $x > 0$ and 0 otherwise and with $J(x) = J_0 + J_1 \cos(x)$ is precisely the model studied in [Roxin et al.(2005)], [Roxin et al.(2006)]. We now wish to study Eq.3 for arbitrary choices of $\Phi(I)$ and $J(x)$.

In presenting Eq.3 we have relied on the heuristic physiological motivation first put forth in [Wilson and Cowan(1972)]. Nonetheless, as a phenomenological model, the terms and parameters in Eq.3 may have alternative and equally plausible interpretations. Indeed, the variable r is often thought of as the firing rate as opposed to the fraction of active cells, in which case the function $\Phi(I)$ can be thought of as the transfer function or fI curve of a cell. Experimentally this function has been found to be well approximated by a power-law nonlinearity with a power greater than one [Miller and Troyer(2002)], [Hansel and van Vreeswijk(2002)]. Modeling studies show that the same nonlinearity applies to integrate-and-fire neurons and conductance based neurons driven by noisy inputs [Hansel and van Vreeswijk(2002)]. Therefore it may be that such a choice of Φ leads to better agreement of Eq.3 with networks of spiking neurons and hence with actual neuronal activity. More fundamentally, we may ask if choosing Φ as a sigmoid or a power law qualitatively alters the dynamical states arising in Eq.3. This is precisely why we choose here not to impose restrictions on Φ but rather conduct an analysis valid for any Φ . How the choice of Φ affects the generation of oscillations and waves is an issue we will return to in the corresponding sections of this paper.

2.1. Linear stability analysis. Stationary uniform solutions (SU) of Eq.3 are given by

$$(4) \quad R = \Phi(J_0 R + I),$$

where R is a constant non-zero rate, J_0 is the zeroth order spatial Fourier coefficient of the symmetric connectivity which can be expressed as

$$(5) \quad J(x) = J_0 + \left(\sum_{k=1}^{\infty} J_k e^{ikx} + c.c. \right)$$

and k is an integer. Depending on the form of Φ , Eq.4 may admit one or several solutions.

We study the linear stability of the SU state with the ansatz

$$(6) \quad r(x, t) = R + \sum_{k=0}^{\infty} \delta r_k e^{ikx + \alpha(k)t},$$

where $\delta r_k \ll 1$ and the spatial wavenumber k is an integer due to the periodic boundary conditions. Plugging Eq.6 into Eq.3 leads to an equation for the complex eigenvalue $\alpha(k)$

$$(7) \quad \alpha(k) = -1 + \Phi' J_k e^{-\alpha(k)D},$$

where the slope Φ' is evaluated at the fixed point given by Eq.4. The real and imaginary parts of the eigenvalue $\alpha(k) = \lambda(k) + i\omega(k)$ represent the linear growth rate and frequency of perturbations with spatial wavenumber k respectively. At the bifurcation of a single mode, the growth rate will reach zero at exactly one point and be negative elsewhere. That is, $\lambda(k_{cr}) = 0$ for the critical mode k_{cr} . Given this, Eq.7 yields the dispersion relation for the frequency of oscillation of the critical mode

$$(8) \quad i\omega(k_{cr}) = -1 + \Phi' J_{k_{cr}} e^{-i\omega(k_{cr})D}.$$

From Eq.8 it is clear that the wavelength of the critical mode depends crucially on the synaptic connectivity. In particular, the spatial Fourier coefficients of the connectivity kernel $J(x)$ depend on the wavenumber k , i.e. $J_k = J(k)$. Thus, the critical wavenumber is, in effect, selected by the choice of connectivity kernel. It is in this way that the nature of the instability depends on the synaptic connectivity at the linear level.

Depending on the values of ω and k_{cr} in Eq.8 at the bifurcation from the SU state, four types of instabilities are possible:

- Steady ($\omega = 0, k_{cr} = 0$): the instability leads to a global increase in activity.
- Turing ($\omega = 0, k_{cr} \neq 0$): the instability leads to a stationary bump state.
- Hopf ($\omega \neq 0, k_{cr} = 0$): the instability leads to an oscillatory uniform state.
- Turing-Hopf ($\omega \neq 0, k_{cr} \neq 0$): the instability leads to waves.

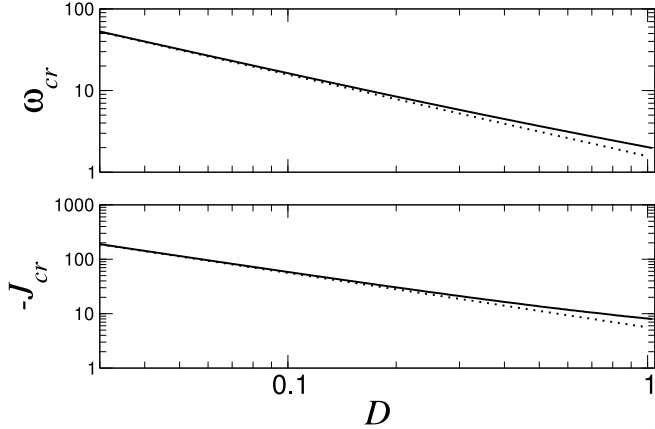


FIGURE 1. Top: The critical frequency of oscillatory instabilities as a function of the delay D from the dispersion equation Eq.10a (solid line) and in the small delay limit (dotted line). Bottom: The critical coupling as a function of the delay D from Eq.10b (solid) and in the small delay limit (dotted).

For the non-oscillatory instabilities (i.e. $\omega = 0$), Eq.8 gives the critical value

$$(9) \quad \bar{J}_k = 1/\Phi'$$

while for the oscillatory ones Eq.8 is equivalent to the system of two transcendental equations

$$(10a) \quad \bar{\omega} = -\tan \bar{\omega}D,$$

$$(10b) \quad \bar{\omega} = -\Phi' \bar{J}_k \sin \bar{\omega}D.$$

Note that we have defined the critical values as $J_{k_{cr}} \equiv \bar{J}_k$ and $\omega_{cr} \equiv \bar{\omega}$.

As fixed delays are on the order of a few milliseconds and the integration time constant is about an order of magnitude larger, the limit of $D \rightarrow 0$ is a relevant one physiologically. This allows us to gain some intuition regarding the effect of fixed delays on the dynamics by deriving asymptotic results in the limit of small delay. Therefore throughout this work we will present asymptotic results, and compare them to the full analytical formulas, as well as numerical simulations. In the limit of small delay $D \rightarrow 0$, it can be easily shown that an instability of the k^{th} spatial Fourier mode occurs at the critical value of the coupling

$$(11) \quad \bar{J}_k = -\frac{\pi}{2D\Phi'},$$

with a frequency

$$(12) \quad \bar{\omega} = \frac{\pi}{2D}.$$

Fig.2.1 shows the critical frequency and coupling as a function of the delay, up to a delay of 1. The solution obtained from the dispersion relation Eqs.10a and 10b

are given by solid lines, while the expressions obtained in the small delay limit are given by dotted lines. Thus the expressions in the small delay limit agree quite well with the full expressions even for $D = 1$.

2.2. An illustrative Phase Diagram. Throughout the analysis which follows we will illustrate our results with a phase diagram of dynamical states. Specifically, we will follow the analysis in [Roxin et al.(2005)], [Roxin et al.(2006)] in constructing a phase diagram of dynamical states as a function of J_0 and J_1 , the first two Fourier coefficients of the synaptic connectivity. We will set the higher order coefficients to zero for this particular phase diagram, although we will discuss the effect of additional modes in the text. Furthermore, unless otherwise noted, for simulations we choose a sigmoidal transfer function $\Phi(I) = \frac{\alpha}{1+e^{-\beta I}}$ with $\alpha = 1.5$ and $\beta = 3$. As we vary the connectivity in the phase diagram, we also vary the constant input I in order to maintain the same level of mean activity, i.e. we keep $R = 0.1$ fixed. For the values of the parameters we have chosen here this results in $I \sim -0.1J_0 - 0.88$. We also take $D = 0.1$ unless noted otherwise

The primary instability lines for the SU state can be seen in the phase diagram, Fig.2. The region in (J_0, J_1) space where the SU state is stable is shown in gray, while the primary instabilities, listed above, are shown as red lines (color online). In Section 3 we will provide a detailed analysis of the bumps, global oscillations and waves (SB, OU and SW/TW) which arise due to the Turing, Hopf and Turing-Hopf instabilities respectively. The derivation of the amplitude equations is given in Appendix A, as well as a brief discussion of the steady, transcritical bifurcation which occurs for strong excitatory coupling and is not of primary interest for this study. Finally, in Section 4 we will analyze the codimension 2 bifurcations: Hopf and Turing-Hopf (OU and waves), and Turing and Hopf (SU and OU). This analysis will allow us to understand the dynamical states which appear near the upper and lower left hand corners of the grey shaded region in Fig.2, i.e. the SW/OU and OB states.

3. BIFURCATIONS OF CODIMENSION 1

As we are interested in creating a phase diagram as a function of the connectivity, we will take changes in the connectivity as the bifurcation parameter. The small parameter ϵ is therefore defined by the expansion

$$(13) \quad J_k = \bar{J}_k + \epsilon^2 \Delta J_k,$$

The perturbative method we apply, which makes use of this small parameter, is called the multiple-scales method and is a standard approach for determining the weakly nonlinear behavior of pattern-forming instabilities, see [Cross and Hohenberg(1993)]. We choose the particular scaling of ϵ^2 in the foreknowledge that if the amplitudes of the patterns of interest are scaled as ϵ , a solvability condition will arise at order ϵ^3 . This solvability condition yields a dynamical equation governing the temporal evolution of the pattern. See Appendix

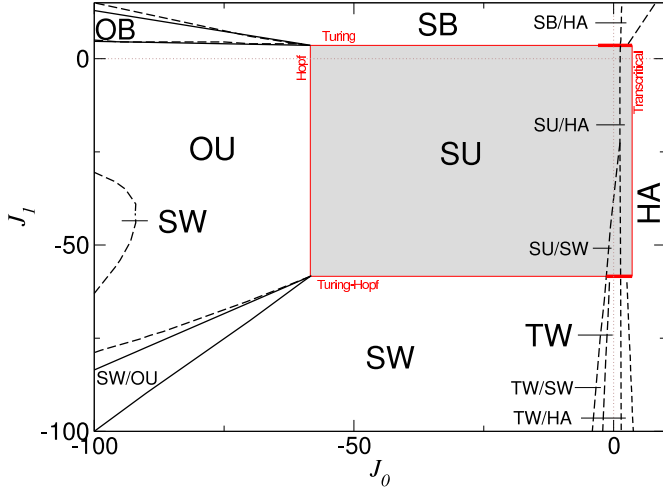


FIGURE 2. (Color online) Phase diagram of the rate model Eq.3. In each region, the type of solution seen in numerical simulations is indicated by a letter code: SU - stationary uniform (grey region), HA - high activity, SB - stationary bump, OB - oscillatory bump, SW - standing waves, TW - traveling waves. Solid lines indicate analytical expressions. In particular, the four possible instabilities of the SU state are depicted in red (thick lines correspond to sub-critical bifurcations) and are given by the linear stability criteria Eqs.9-10b. The four lines emanating from the upper and lower left corners of the SU region were determined from a weakly nonlinear analysis at the two corners (codimension two points), see section IV. The region marked OB corresponds to a mixed mode solution of SB-OU, while in the lower left-hand region the OU and SW solutions are bistable. Parameters: $\Phi(x) = \frac{\alpha}{1+e^{-\beta x}}$ where $\alpha = 1.5$ and $\beta = 3$. We consider the coupling function $J(x) = J_0 + 2J_1 \cos x$. The time delay is $D = 0.1$ and the input current I is varied so as to keep the uniform stationary solution fixed at $R = 0.1$.

A for details. Without loss of generality we will assume that an instability of a nonzero spatial wavenumber is for $k = 1$. We will furthermore co-expand the constant input I so as to maintain a fixed value for the spatially homogeneous steady state solution R

$$(14) \quad I = \bar{I} + \epsilon^2 \Delta I,$$

$$(15) \quad r = R + \epsilon r_1 + \epsilon^2 r_2 + \dots,$$

where the small parameter ϵ is defined by Eq.13. Additionally we define the slow time

$$(16) \quad T = \epsilon^2 t.$$

3.1. Turing Bifurcation: $\omega = 0$, $k \neq 0$. The emergence and nature of stationary bumps in rate equations have been extensively studied elsewhere, e.g. [Ermentrout and Cowan(1980)]. We briefly describe this state here for completeness. The k^{th} spatial Fourier mode of the connectivity is given by the critical value Eq. 9, while we assume that all other Fourier modes are sufficiently below their critical values to avoid additional instabilities. Without loss of generality we assume $k = 1$ here.

We expand the parameters J_1 , I and r as in Eqs. 13,14,15, and define the slow time Eq. 16. The solution of Eq.3 linearized about the SU state R is a spatially periodic amplitude which we allow to vary slowly in time, i.e. $r_1 = A(T)e^{ix} + c.c.$. Carrying out a weakly nonlinear analysis to third order in ϵ leads to the amplitude equation

$$(17) \quad \partial_T A = \eta \Delta J_k A + \Gamma |A|^2 A,$$

with the coefficients

$$(18a) \quad \eta = \frac{\Phi'}{1+D},$$

$$(18b) \quad \Gamma = \frac{\bar{J}_1^3}{1+D} \left(\frac{J_0(\Phi'')^2}{1-J_0\Phi'} + \frac{J_2(\Phi'')^2}{2(1-J_2\Phi')} + \frac{\Phi'''}{2} \right).$$

The nature of the bifurcation (sub- or supercritical) clearly depends strongly on the sign and magnitude of mean connectivity J_0 and the second spatial Fourier mode J_2 . Fig.3 shows a phase diagram of the bump state at the critical value of $\bar{J}_1 = 3.54$. The red lines indicate oscillatory and steady instability boundaries for the modes J_0 and J_2 . Clearly $J_0 < 0$ and $J_2 < 0$ over most of the region of allowable values, and the bump is therefore supercritical. There is only a narrow region of predominantly positive values (shaded region in Fig.3) for which the cubic coefficient is positive. This indicates that the bifurcating solution branch is unstable. However, neuronal activity is bounded, which is captured in Eq.3 by a saturating transfer function Φ . Thus the instability will not grow without bound but rather will saturate, producing a finite amplitude bump solution. This stable, large amplitude branch and the unstable branch annihilate in a saddle-node bifurcation for values of J_1 below the critical value for the Turing instability. Such finite-amplitude bumps are therefore bistable with the SU state. In Fig.3, the two insets show the connectivity kernel $J(x)$ for parameter values given by the placement of the open triangle (subcritical bump) and the open square (supercritical bump).

In the phase diagram Fig.2, the Turing instability line (upper horizontal red line) is shown thin for supercritical, and thick for subcritical bumps (here $J_2 = 0$).

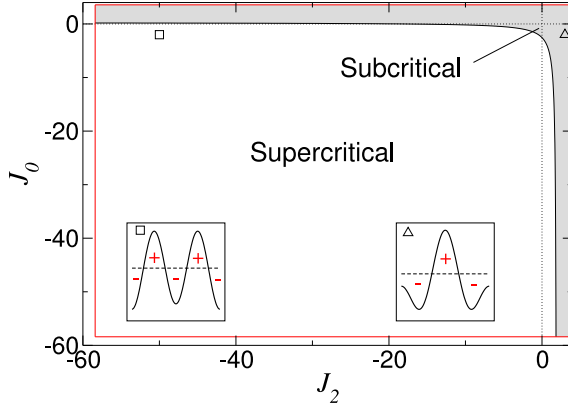


FIGURE 3. (Color online) The phase diagram for stationary bumps as a function of the zeroth and second spatial Fourier modes of the connectivity kernel. The region of bistability between the unpatterned and the bump state is shaded. Here the critical spatial Fourier coefficient $\bar{J}_1 = 3.54$. Red lines indicate the boundaries of the SU state (obtained via Eqs.9-10b). The functions Φ and $J(x)$ as well as the input current I and the delay D are taken as in Fig.2. Insets: example connectivity patterns corresponding to the values of J_0 and J_2 marked by the square and triangle respectively. Note that standard Mexican Hat connectivity tends to favor bistability.

3.2. Hopf Bifurcation: $\omega \neq 0, k = 0$. There is a spatially homogeneous oscillatory instability with frequency ω given by Eq.10a. This occurs for a value of the 0^{th} spatial Fourier mode of the connectivity given by Eq.10b, while we assume that all other Fourier modes are sufficiently below their critical values to avoid additional instabilities. We expand the parameters J_0, I and r as in Eqs. 13,14,15, and define the slow time Eq. 16. The linear solution has an amplitude which we allow to vary slowly in time, i.e. $r_1 = H(T)e^{i\omega t} + c.c.$. Carrying out a weakly nonlinear analysis to third order in ϵ leads to the amplitude equation

$$(19) \quad \partial_T H = (\mu + i\Omega)\Delta J_0 H + (\alpha + i\beta)|H|^2 H,$$

where the coefficients $(\mu + i\Omega)$ and $(\alpha + i\beta)$ are specified by the Eqs.51 and 52 in the Appendix.

Fig.4 shows a typical bifurcation diagram (in this case $J_1 = 0$) for the Hopf bifurcation. Plotted is the amplitude of the limit cycle as a function of J_0 where symbols are from numerical simulation of Eq.3 and the lines are from the amplitude equation, Eq.19.

In the small delay limit ($D \rightarrow 0$) we can use the asymptotic values Eqs.12 to obtain, to leading order,

$$(20a) \quad \mu + i\Omega = -\frac{\left(\frac{\pi}{2} + i\right)\Phi'}{1 + \frac{\pi^2}{4}},$$

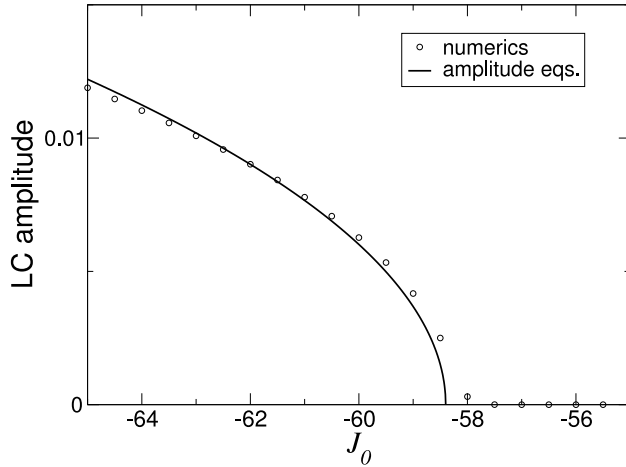


FIGURE 4. The bifurcation diagram for a supercritical Hopf bifurcation. Shown is the amplitude of the limit cycle as a function of the 0th order spatial Fourier coefficient of the coupling $J(x)$. Open circles are from numerical simulation of Eq.3 and solid lines show the solution from the amplitude equation, Eq.17. The functions Φ and $J(x)$ as well as the input current I and the delay D are taken as in Fig.2.

$$\alpha + i\beta = -\frac{\chi}{(D\Phi')^3} \left(\frac{(11\pi - 4)(\Phi'')^2}{20} \frac{\Phi'''}{\Phi'} - \frac{\pi\Phi'''}{4} - i \left[\frac{(11 + \pi)}{10} - \frac{\Phi'''}{2} \right] \right), \quad (20b)$$

where we have defined the quantity $\chi \equiv \pi^3/(8 + 2\pi^2)$.

Fig.5 shows a comparison of the full expressions for the coefficients of the amplitude equation, Eqs.51-52 with the expressions obtained in the limit $D \rightarrow 0$, Eqs.20a -20b. Again, the agreement is quite good, even up to $D = 1$, especially for the real part of the cubic coefficient α , which is of primary interest here. The asymptotic expression for the cubic coefficient α , Eq.20b, indicates that a subcritical limit cycle should occur for $\Phi''\Phi' / (\Phi'')^2 > (11\pi - 4)/(5\pi)$. This provides a simple criterion for determining whether or not a particular choice of the transfer function can generate oscillations which are bistable with the SU state. In fact, it is a difficult condition to fulfill given a sigmoidal-like input-output function. For example, given a sigmoid of the form $\Phi(x) = \alpha/(1 + e^{-\beta x})$, one finds that

$$(21) \quad \frac{\Phi'''\Phi'}{(\Phi'')^2} = 1 - 2 \frac{e^{-3\beta x}}{(e^{-4\beta x} - 2e^{-3\beta x} + e^{-2\beta x})}.$$

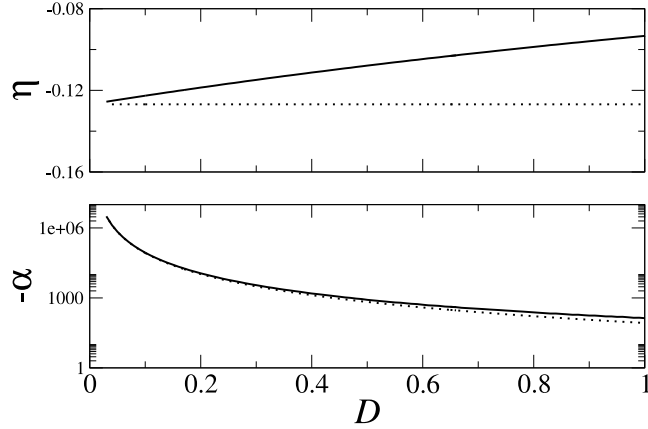


FIGURE 5. Top: The real part of the linear coefficient μ . Bottom: Minus the real part of the cubic coefficient $-\alpha$. Solid lines are from the full expressions Eq.51-52 and dotted lines are the leading order terms in the small delay limit, Eqs.20a-20b. The functions Φ and $J(x)$ as well as the input current I are taken as in Fig.2.

It is straightforward to show that Eq.21 is bounded above by 1. In fact, $-\infty \leq \Phi'''\Phi' / (\Phi'')^2 < 1 < (11 - 4\pi)/(5\pi) \sim 1.95$. Such a nonlinear transfer function will therefore always generate supercritical oscillations.

If the nonlinear transfer function is interpreted as the single-cell fI curve, which is common in the literature, then we can use the fact that cortical cells operate in the fluctuation-driven regime. In particular, the mean input current to cortical cells is too low to cause spiking. Rather, this occurs at very low rates due to fluctuations in the membrane voltage. Although the fI curve for spiking neurons in the supra-threshold regime is concave down and saturates, in the fluctuation-driven, sub-threshold regime the fI curve exhibits a smoothed out tail which is concave up. It has been shown that the sub-threshold portion of the fI curve of actual cells can be well fit by a function of the form $\Phi(x) = Ax^\gamma$, where $\gamma > 1$, see e.g. [Miller and Troyer(2002)], [Hansel and van Vreeswijk(2002)]. It is straightforward to show that in this case

$$\frac{\Phi'''\Phi'}{(\Phi'')^2} = 1 - \frac{1}{\gamma - 1},$$

which again is bounded between $-\infty$ and 1. This again rules out subcritical oscillations in the small delay limit. Nonetheless, suitable functions Φ for generating subcritical oscillations can be contrived, as shown in Fig.6A. Numerical simulation of Eq.3 indeed reveals a subcritical bifurcation in this case, see Fig.6B. However, this type of transfer function does not seem consistent with the interpretation of Φ as a single-cell fI curve, nor with that of Φ as a cumulative distribution of activation, i.e. a sigmoid. This strongly suggests that delay-driven oscillations in networks of spiking neurons will be generically supercritical. This

is consistent with the result of a weakly nonlinear analysis of a Hopf instability in a network of integrate-and-fire neurons [Brunel and Hakim(1999)] and with numerical simulations of Hodgkin-Huxley neurons [Roxin et al.(2005)].

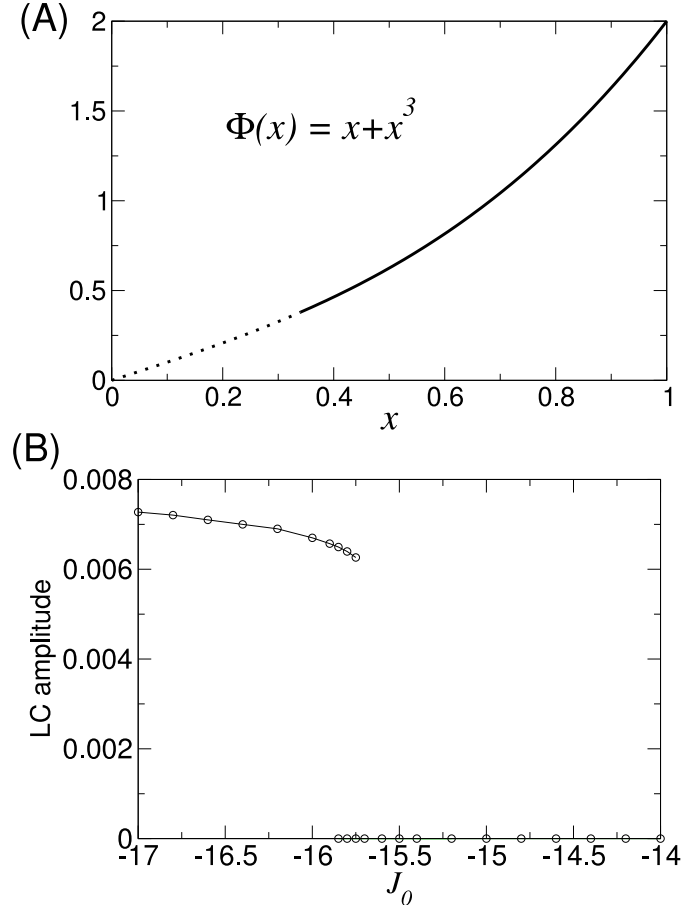


FIGURE 6. A. An example of a function $\Phi(x)$ for which subcritical oscillations are possible. The dotted curve indicates the range of the function Φ over which oscillations are subcritical. B. A bifurcation diagram for subcritical oscillations when the function $\Phi(x)$ is the same as in panel A. Open circles: the limit cycle amplitude computed numerically as a function of J_0 . Here $D = 0.1$ and the critical coupling is $\bar{J}_0 = -15.89$. The fixed point is held at $R = 0.1$ and thus the value of x in panel A is close to 0.1 ($x + x^3 = 0.1$).

3.3. Turing-Hopf Bifurcation: $\omega \neq 0$, $k \neq 0$. There is a spatially inhomogeneous oscillatory instability with frequency ω given by Eq.10a. This occurs for a value of the k^{th} spatial Fourier mode of the connectivity given by Eq.10b, while we assume that all other Fourier modes are sufficiently below their critical values to avoid additional instabilities. Without loss of generality we assume $k = 1$.

We expand the parameters J_1 , I and r as in Eqs. 13,14,15, and define the slow time Eq. 16. The linear solution consists of leftwards and rightwards traveling waves with an amplitude which we allow to vary slowly in time, i.e. $r_1 = A(T)e^{i\omega t+ix} + B(T)e^{-i\omega t+ix} + c.c.$. Carrying out a weakly nonlinear analysis to third order in ϵ leads to the coupled amplitude equations

$$(22a) \quad \partial_T A = (\mu + i\Omega)\Delta J_1 A + (a + ib)|A|^2 A + (c + id)|B|^2 A,$$

$$(22b) \quad \partial_T B = (\mu - i\Omega)\Delta J_1 B + (a - ib)|B|^2 B + (c - id)|A|^2 B,$$

where the coefficients $(a + ib)$, $(c + id)$ and $(\mu + i\Omega)$ are given by the Eqs.55, 56 and 51, respectively.

In the small delay limit ($D \rightarrow 0$) we can use the asymptotic values Eqs.12 to obtain, to leading order,

$$(23a) \quad a + ib = \frac{\chi(\frac{\pi}{2} + i)}{(D\Phi')^3} \left(\frac{J_0(\Phi'')^2}{1 - \Phi' J_0} + \frac{\Phi'''}{2} \right),$$

$$(23b) \quad c + id = \frac{\chi(\frac{\pi}{2} + i)}{(D\Phi')^3} \left(\frac{J_0(\Phi'')^2}{1 - \Phi' J_0} + \Phi'''' + \frac{J_2(\Phi'')^2}{1 - \Phi' J_2} \right).$$

Fig.7 shows a comparison of the full expressions (solid lines) for the real parts of the cubic and cross-coupling coefficients a and c with the asymptotic expressions above (dotted lines).

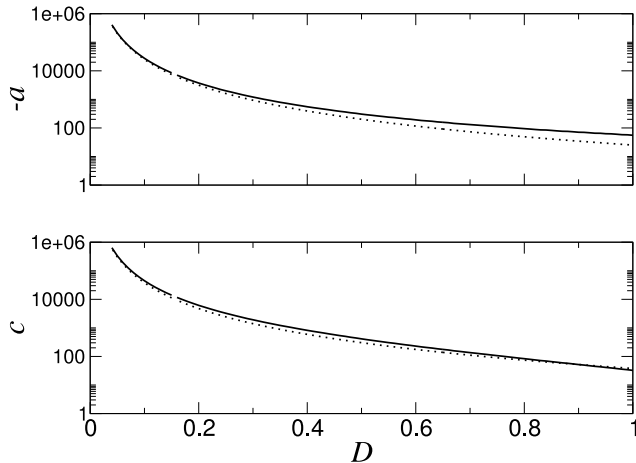


FIGURE 7. Top: The real part of the cubic coefficient a . Bottom: The real part of the cross-coupling coefficient c . Solid lines are from the full expressions Eq.55-56 and dotted lines are the leading order terms in the small delay limit, Eqs.23a-23b. The functions Φ and $J(x)$ as well as the input current I are taken as in Fig.2.

3.3.1. Wave solutions and their stability. Eqs.22a and 22b admit solutions of the form $(A, B) = (\mathcal{A}e^{i\theta_A}, \mathcal{B}e^{i\theta_B})$, where the amplitudes \mathcal{A} and \mathcal{B} obey

$$(24a) \quad \dot{\mathcal{A}} = \mu\Delta J_1 \mathcal{A} + a\mathcal{A}^3 + c\mathcal{B}^2 \mathcal{A},$$

$$(24b) \quad \dot{\mathcal{B}} = \mu\Delta J_1 \mathcal{B} + a\mathcal{B}^3 + c\mathcal{A}^2 \mathcal{B}.$$

Traveling waves: Leftward and rightward traveling waves in Eqs. 24a and 24b are given by $(\mathcal{A}_{TW}, 0)$ and $(0, \mathcal{A}_{TW})$ respectively, where $\mathcal{A}_{TW} = -\mu\Delta J_1/a$. The stability of traveling waves can be determined with the ansatz $(\mathcal{A}, \mathcal{B}) = (\mathcal{A}_{TW}, 0) + (\delta\mathcal{A}, \delta\mathcal{B})e^{\lambda t}$. The resulting eigenvalues are $\lambda_1 = -2\mu\Delta J_1$ and $\lambda_2 = -\mu\Delta J_1(c/a - 1)$.

Standing waves: Standing waves in Eqs.24a and 24b are given by $(\mathcal{A}_{SW}, \mathcal{A}_{SW})$, where $\mathcal{A}_{TW} = -\mu\Delta J_1/(a+c)$. The stability of standing waves can be determined with the ansatz $(\mathcal{A}, \mathcal{B}) = (\mathcal{A}_{SW}, \mathcal{A}_{SW}) + (\delta\mathcal{A}, \delta\mathcal{B})e^{\lambda t}$. The resulting eigenvalues are $\lambda_1 = -2\mu\Delta J_1$ and $\lambda_2 = -2\mu\Delta J_1(a - c)/(a + c)$.

The existence and stability of small-amplitude waves as described above is completely determined by the values of the cubic and cross-coupling coefficients a and c . This is illustrated in Fig.8, where the parameter space is divided into five sectors. In each sector the type of solution which will be observed numerically is indicated where known, and otherwise a question mark is placed. Illustrative bifurcation diagrams are also given. Specifically, in the region labeled 1 (red online), the SW solution is supercritical and unstable while the TW solution is supercritical and stable. TW will therefore be observed. In the region labeled 2, the SW solution is supercritical and unstable while the TW solution is subcritical. Finite-amplitude TW are therefore expected to occur past the bifurcation point. In the region labeled 3, both solution branches are subcritical, indicating that the analysis up to cubic order is not sufficient to identify the type of wave which will be observed. In the region labeled 4, TW are supercritical and unstable while SW are subcritical. Finite amplitude SW are therefore expected past the bifurcation point. In the region labeled 5, the TW solution is supercritical and unstable while the SW solution is supercritical and stable. SW will therefore be observed.

In the small delay limit, we find, from Eqs.23a-23b, that

$$(25) \quad a = c - \frac{\pi}{2} \frac{\chi}{(D\Phi)^3} \left(\frac{\Phi'''}{2} + \frac{J_2(\Phi'')^2}{1 - \Phi' J_2} \right).$$

It is clear from Fig.8 that the nature of the solution seen will depend crucially on the sign of the second term of the right-hand side of Eq.25. In particular, the diagonal $a = c$ divides the the parameter space into two qualitatively different regions. Above this line TWs are favored while below it SWs are favored. In the small delay limit, Eq.25 indicates that the balance between the third derivative of

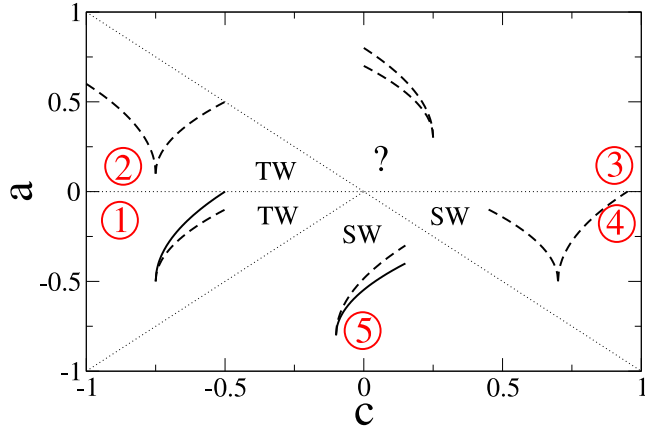


FIGURE 8. The existence and stability of traveling and standing waves as a function of the cubic and cross-coupling coefficients a and c . In each sector of parameter space a representative bifurcation diagram is shown. Supercritical (subcritical) solutions are shown growing from left to right (right to left). Stable (unstable) solutions are given by solid (dashed) lines. Also indicated in each sector is the type of solution which will be seen numerically. A question mark is placed wherever the type of stable solution cannot be determined through a weakly nonlinear analysis.

the transfer function Φ'' and the second spatial Fourier mode of the connectivity kernel will determine whether TW or SW are favored.

For sigmoidal transfer functions, the third derivative changes sign from positive to negative already below the inflection point, while for expansive power-law nonlinearities, which fit cortical neuronal responses quite well in the fluctuation-driven regime, the third derivative is positive if the power is greater than 2 and is negative otherwise. The contribution of this term therefore will depend on the details of the neuronal response. In simulations of large networks of conductance-based neurons in the fluctuation-driven regime in which J_2 was zero, the standing wave state was always observed, indicating a $\Phi'' > 0$ [Roxin et al.(2005)], [Roxin et al.(2006)].

The phase diagram for $J_2 = 0$, Fig.2, clearly shows the dominance of the SW solution, indicating $\Phi'' > 0$ for the parameter values chosen. Specifically, for values of $J_0 < -6.3$, supercritical standing waves are stable, see region 5 in Fig.8. Fig.9A and Fig.9B show supercritical SW patterns for $J_0 = -40$ and $J_0 = -9$ respectively. For $-6.3 < J_0 < -2.6$ TW are supercritical and unstable while SW are subcritical, see region 4 in Fig.8. An example of subcritical SW is shown in Fig.9C. For $-2.6 < J_0 < 3.58$ both SW and TW are subcritical, see region 3 in Fig.8. Numerical simulations reveal TW patterns in this region, see an example in Fig.9D. In the region where SW are subcritical there is a small sliver in (J_0, J_1)

where the SW state is bistable with a TW state (TW/SW in the phase diagram). This TW branch most likely arises in a secondary bifurcation slightly below the Turing-Hopf bifurcation line. There is also a small region of bistability between large amplitude TW and the spatially uniform high activity state (TW/HA in the phase diagram Fig.2).

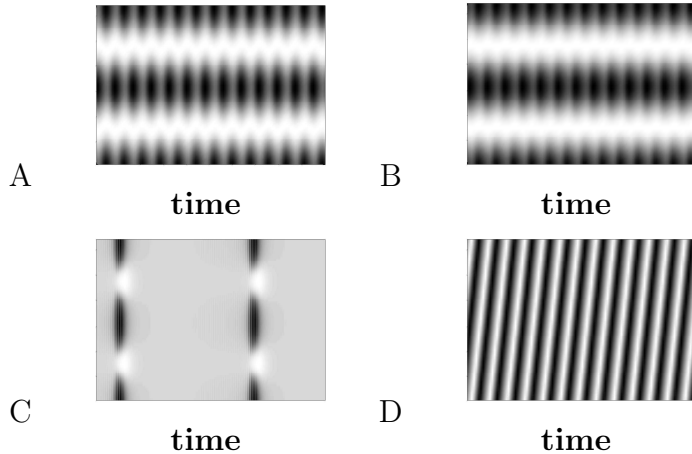


FIGURE 9. Examples of wave solutions from numerical simulation of Eq.3. The functions Φ and $J(x)$ as well as the input current I and the delay D are taken as in Fig.2, with $J_1 = -120$. A. Supercritical standing waves: $J_0 = -40$ and 5 units of time are shown. B. Supercritical standing waves: $J_0 = -9$ and 5 units of time are shown. C. Subcritical standing waves: $J_0 = -5$ and 40 units of time are shown. D. Subcritical traveling waves: $J_0 = 0$ and 5 units of time are shown.

Thus for $\Phi'' > 0$ and with a simple cosine connectivity, SW arise for most values of J_0 . However, adding a non-zero J_2 can lead to the TW solution winning out. The phase diagram of wave states as a function of J_0 and J_2 is shown in Fig.3.3.1A. In Fig.3.3.1A, the light shaded region indicates values of J_0 and J_2 for which TW are expected, whereas SW are expected in the dark shaded region. In the unshaded region, both TW and SW are subcritical and the solution type is therefore not determined by the analysis up to cubic order. These regions, delimited by the solid lines, were determined by numerically evaluating the real parts of the full expressions for the cubic and cross-coupling coefficients, Eqs.55-56. Each region is furthermore numbered according to the existence and stability of the TW and SW solution branches as shown in Fig.8. The dashed lines show the approximation to the solid lines given by the asymptotic formulas Eqs.23a-23b. The set of allowable values for J_0 and J_2 is bounded by the conditions for a steady or oscillatory linear instability Eqs.9-10b. These stability conditions are shown by the horizontal and vertical bounding lines (red online).

All parameter values are as in Fig.2. From Fig.3.3.1 we can now understand the discrepancy between the analytical results in [Roxin et al.(2005)] using a rate equation with a linear threshold transfer function, which predicted TW, and network simulations, which showed SW. Specifically, given a nonlinear transfer function with $\Phi''' > 0$, then with a simple cosine coupling SW are predicted over almost the entire range of allowable J_0 (dark shaded region for $J_2 = 0$). The nonlinear transformation of inputs into outputs is thus crucial in determining the type of wave solution. The choice of a threshold linear transfer function results in the second and all higher order derivatives being zero. In this sense it produces degenerate behavior at a bifurcation point, and by continuation of the solution branches, in a finite region of the phase diagram.

We have shown that varying J_0 can change the nature of the bifurcation, e.g. supercritical to subcritical, while varying J_2 can switch the solution type, e.g. from SW to TW. As an example of a functional form of connectivity motivated by anatomical findings, e.g. [Hellwig(2000)], we consider a difference of Gaussians, written as

$$(26) \quad J(x) = \frac{J_e}{\sqrt{2\pi}\sigma_e} e^{-\frac{x^2}{2\sigma_e^2}} - \frac{J_i}{\sqrt{2\pi}\sigma_i} e^{-\frac{x^2}{2\sigma_i^2}}.$$

In this case, one finds that the Fourier coefficients are

$$(27) \quad J_k = J_e e^{-k^2\sigma_e^2/2} f(k, \sigma_e) - J_i e^{-k^2\sigma_i^2/2} f(k, \sigma_i).$$

where $f(k, \sigma_{e,i}) = \text{Re}[\text{Erf}((\pi/\sigma_{e,i} + ik^2)/\sqrt{2})]/\pi$. Once J_1 has been fixed at the critical value for the onset of waves, from Eq.27 it is straightforward to show that $J_0 = -pJ_2 + q$ where both p and q are constants which depend on σ_e and σ_i , the widths of the excitatory and inhibitory axonal projections respectively. Thus a difference-of-Gaussian connectivity, constrains the possible values of J_0 and J_2 to lie along a straight line for fixed connectivity widths. This is illustrated in Fig.3.3.1B where three dashed lines are superimposed on the phase diagram, corresponding to the values $\sigma_{e,i} = (1.5, 1.49)$; $\sigma_{e,i} = (1, 0.99)$; and $\sigma_{e,i} = (0.7, 0.69)$. Each of these lines is bounding a region to the left where σ_e and σ_i are less than 0.7, 1.0 and 1.5 respectively. Given periodic boundary conditions with a system size of 2π , a Gaussian with $\sigma = 1.5$ is already significantly larger than zero for $x = \pi$ or $-\pi$. Thus, restricting ourselves to Gaussians which essentially decay to zero at the boundaries means that TW will always be observed. The same holds true for qualitatively similar types of connectivity.

3.3.2. Waves in Network Simulations. Our analytical results concerning waves from the rate equation Eq.3 predict that a connectivity with a sufficiently strong second Fourier component with a negative amplitude will lead to traveling waves. We can test this prediction in simulations of networks of spiking neurons. In doing so we use the same general network as in earlier work [Roxin et al.(2005)], [Roxin et al.(2006)] but with modified connectivity. Briefly, we consider two populations of $N = 2000$ conductance based neurons each, arranged on a ring. We use

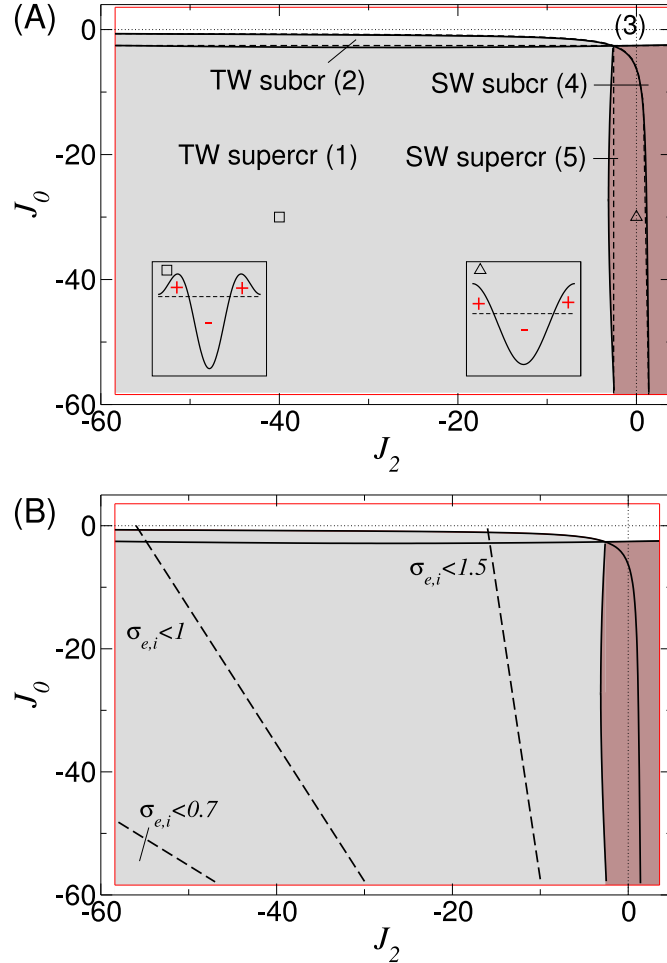


FIGURE 10. (Color online) A. Phase diagram for waves as a function of the zeroth and second spatial Fourier coefficients of the connectivity kernel. The dark-shaded region indicates SW, whereas the light shaded region indicates TW. Red lines indicate boundaries for primary instabilities of J_0 and J_2 given by Eqs.9-10b. Solid stability lines for waves are from Eqs.55-56 while the dashed line are from the asymptotic expressions, Eqs.23a-23b. Here $\bar{J}_1 = -58.4$. The function Φ as well as the input current I and the delay D are taken as in Fig.2. Insets: example connectivity patterns corresponding to the values of J_0 and J_2 marked by the square and triangle respectively. B. The same phase diagram as in A, now showing where various types of ‘difference-of-Gaussian’ connectivities, Eq. 26, would lie. Each dotted line indicates the border of a region in which the standard deviations of the excitatory and inhibitory connectivities are below a certain threshold (0.7, 1.0 and 1.5 respectively, see text). Relatively narrow connectivities compared to the system size will always generate TW solutions. See text for details.

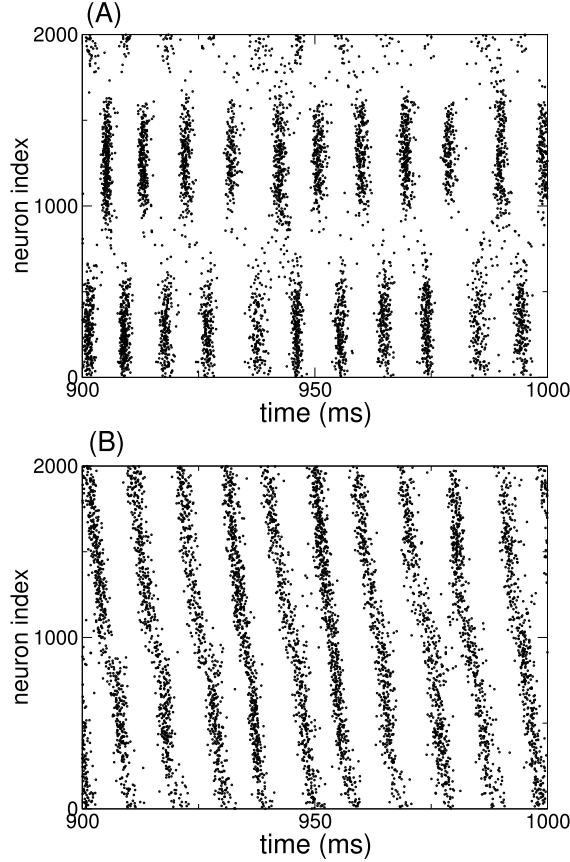


FIGURE 11. Raster plots of spiking activity in a network of conductance-based neurons. A. Standing waves. Parameters are the same as in Fig.3 [Roxin et al.(2005)], right column, third down. $p_E = 0.2$, $p_I = 0.2 + 0.2 \cos r$. B. Traveling waves. $p_E = 0.2$, $p_I = 0.2 + 0.2 \cos r + 0.1 \cos 2r$. $g_E = 0.01$, $g_I = 0.028$, $g_{ext} = 0.001$, $\nu_{ext} = 5000$.

a Hodgkin-Huxley formalism with one somatic compartment. Action potentials are shaped by Na and K. For details of the model see [Wang and Buzsáki(1996)]. The probability of connection from a neuron in population $A (= E, I)$ to a neuron in population $B (= E, I)$ is $p_{BA} = p_0^{BA} + p_1^{BA} \cos r + p_2^{BA} \cos 2r$, where r is the distance between the two neurons. Here we take $p_i^{BA} = p_i^A$, i.e. the excitatory and inhibitory input is the same for both excitatory and inhibitory neurons on average. This leads to one effective population of neurons, the appropriate condition for comparing to Eq.3. Synaptic currents are modeled as $I_{syn,A} = -g_A s(t)(V - V_A)$, $A \in E, I$ where $s(t)$ is modeled as the difference of exponentials with time constants equal to one and three milliseconds respectively, V is the post-synaptic voltage and V_A is the reversal potential and is 0 mV and -80 mV for excitatory and inhibitory synapses respectively. A post-synaptic response $s(t)$ is initiated

whenever a pre-synaptic action-potential reaches 0 mV, with no delay. All the neurons are subjected to an external excitatory input comprised of synaptic activations ($I_{syn,E}$ as defined above) with Poisson statistics at a rate ν_{ext} . Fig.3.3.1 shows the results of the simulations. As predicted the addition of the second spatial Fourier component to the inhibitory connections converts SW into TW.

4. BIFURCATIONS OF CODIMENSION 2

For certain connectivity kernels we may be in the vicinity of two distinct instabilities. This is the case for certain Mexican hat connectivities (OU and SB) and certain inverted Mexican hat connectivities (OU and SW/TW). Although two instabilities will co-occur only at a single point in the phase diagram Fig.2, i.e. J_0 and J_1 are both at their critical values, the competition between these instabilities may lead to solutions which persist over a broad range of connectivities. This is the case here. We can investigate this competition once again using a weakly nonlinear approach. The main results of this section are summarized in table 1.

4.1. Hopf and Turing-Hopf bifurcations. Here we consider the co-occurrence a spatially homogeneous oscillation and a spatially inhomogeneous oscillation (OU and SW/TW), both with frequency ω given by Eq.10a. This instability occurs when the zeroth and k^{th} spatial Fourier mode of the connectivity both satisfy the relation, Eq.10b, while we assume that all other Fourier modes are sufficiently below their critical values to avoid additional instabilities. Without loss of generality we take $k = 1$ for the SW/TW state.

We expand the parameters J_0 , J_1 , I and r as in Eqs. 13,14,15, and define the slow time Eq. 16. The linear solution consists of homogeneous, global oscillations, leftwards and rightwards traveling waves with amplitudes which we allow to vary slowly in time, i.e. $r_1 = H(T)e^{i\omega t} + A(T)e^{i\omega t+ix} + B(T)e^{-i\omega t+ix} + c.c..$ Carrying out a weakly nonlinear analysis to third order in ϵ leads to the coupled amplitude equations

$$(28a) \quad \begin{aligned} \partial_T H &= (\mu + i\Omega)\Delta J_0 H \\ &\quad + 2(\alpha + i\beta)[(\frac{|H|^2}{2} + |A|^2 + |B|^2)H + \bar{H}AB], \end{aligned}$$

$$(28b) \quad \begin{aligned} \partial_T A &= (\mu + i\Omega)\Delta J_1 A + (a + ib)|A|^2 A + (c + id)|B|^2 A \\ &\quad + (\alpha + i\beta)[2|H|^2 A + H^2 B], \end{aligned}$$

$$(28c) \quad \begin{aligned} \partial_T B &= (\mu - i\Omega)\Delta J_1 B + (a - ib)|B|^2 B + (c - id)|A|^2 B \\ &\quad + (\alpha - i\beta)[2|H|^2 B + \bar{H}^2 A], \end{aligned}$$

where $\alpha + i\beta$, $a + ib$ and $c + id$ are given by Eqs.52, 55 and 56, respectively. The overbar in \bar{H} represents the complex conjugate.

4.1.1. Solution types and their stability. Eqs. 28a-28c admit several types of steady state solutions including oscillatory uniform solutions (OU), traveling waves (TW), standing waves (SW) and mixed mode oscillations/standing waves (OU-SW). The stability of these solutions depends on the values of the coefficients in Eqs.28a-28c. In addition, non-stationary solutions are also possible. Here we describe briefly some stationary solutions and their stability. For details see Appendix A.

Oscillatory Uniform (OU): The oscillatory uniform solution has the form $(H, A, B) = (\mathcal{H}e^{i\omega t}, 0, 0)$ where

$$\begin{aligned}\mathcal{H} &= \sqrt{\frac{-\mu\Delta J_0}{\alpha}}, \\ \omega &= \left(\Omega - \frac{\beta\mu}{\alpha}\right)\Delta J_0.\end{aligned}$$

The OU state undergoes a steady instability along the line

$$(29) \quad \Delta J_1 = \Delta J_0.$$

This stability line agrees very well with the results of numerical simulations of Eq.3, see the phase diagram Fig.2.

Traveling Waves (TW): The traveling wave solution has the form $(H, A, B) = (0, \mathcal{A}_{TW}e^{i\omega t}, 0)$ or $(0, 0, \mathcal{A}_{TW}e^{-i\omega t})$, where

$$\begin{aligned}\mathcal{A}_{TW} &= \sqrt{\frac{-\mu\Delta J_1}{a}}, \\ \omega &= \left(\Omega - \frac{b\mu}{a}\right)\Delta J_1.\end{aligned}$$

The TW state undergoes an oscillatory instability along the line

$$(30) \quad \Delta J_1 = \frac{a}{2\alpha}\Delta J_0,$$

with a frequency

$$\bar{\omega} = \left(\Omega(1 - \frac{a}{2\alpha}) + (b - 2\beta)\frac{\mu}{2\alpha}\right)\Delta J_0.$$

Standing Waves (SW): The standing wave solution has the form $(H, A, B) = (0, \mathcal{A}_{SW}e^{i\omega t}, \mathcal{A}_{SW}e^{-i\omega t})$, where

$$(31) \quad \mathcal{A}_{SW} = \sqrt{\frac{-\mu\Delta J_1}{(a+c)}},$$

$$(32) \quad \omega = \left(\Omega - \frac{(b+d)}{(a+c)}\mu\right)\Delta J_1.$$

An oscillatory instability occurs along the line

$$(33) \quad \Delta J_1 = \frac{(a+c)}{4\alpha} \Delta J_0,$$

with a frequency

$$\bar{\omega} = \sqrt{\left[\Omega\left(\frac{a+c}{4\alpha} - 1\right) - \mu\frac{b+d-4\beta}{4\alpha}\right]^2 - \mu^2\frac{\alpha^2 + \beta^2}{4\alpha^2}} \Delta J_0.$$

A stationary instability occurs along the line

$$(34) \quad \Delta J_1 = \Psi \Delta J_0,$$

where

$$\begin{aligned} \Psi &= \frac{-k_2 + \sqrt{k_2^2 - 4k_1k_3}}{2k_1}, \\ k_1 &= \left[\Omega - \mu\frac{(b+d-4\beta)}{(a+c)}\right]^2 + \mu^2\frac{(12\alpha^2 - 4\beta^2)}{(a+c)^2}, \\ k_2 &= -8\mu^2\frac{\alpha}{(a+c)} - 2\Omega^2 + 2\Omega\mu\frac{(b+d-4\beta)}{(a+c)}, \\ k_3 &= \mu^2 + \Omega^2. \end{aligned}$$

For Eq.3 with the parameters used to generate the phase diagram, Fig.2 we find that the stationary instability precedes the oscillatory one and that $\Psi \sim 0.6$. This agrees well with the numerically determined stability line near the co-dimension 2 point, see Fig.2.

Mixed Mode: We can study the mixed mode solutions in Eqs.28a-28c by assuming an ansatz

$$(36) \quad (H, A, B) = (\mathcal{H}e^{i\theta}, \mathcal{A}e^{i\psi_A}, \mathcal{B}e^{-i\psi_B}),$$

which leads to four coupled equations, see Appendix A. We do not study the stability of mixed mode solutions in this work.

4.1.2. A simple example. We now turn to a simple example in order to illustrate the two main types bifurcation scenarios that can arise when small amplitude waves and oscillations interact in harmonic resonance.

i. Bistability: Here we take the parameters ¹. Given these parameter values one finds, from the analysis above, that the oscillatory uniform state has an amplitude $\mathcal{H} = 1$ and destabilizes along the line $\Delta J_k = -1$. The standing wave solution (traveling waves are unstable, see Fig.8) has an amplitude $\mathcal{A}_{SW} = \sqrt{-\Delta J_k}$ which undergoes a steady bifurcation to the oscillatory uniform state at $\Delta J_k = -1/2$. Both solutions are therefore stable in the region $-1 < \Delta J_k < -1/2$. This analysis is borne out by numerical simulation of Eqs.28a-28c, see Fig.12a. Solid and dotted lines are the analytical expressions for the stable and unstable solution branches

¹ $\mu = -1, \Delta J_0 = -1, \alpha = -1, a = -1, b = c = d = \beta = \omega = \Omega = 0$

respectively (red is OU and black is SW). Circles are from numerical simulation of the amplitude equations Eqs.28a -28c.

Note that this scenario is the relevant one for the phase diagram shown in Fig.2. That is, we find there is a region of bistability between the OU and SW solutions, bounded between two lines with slope ~ 0.6 and 1 respectively.

ii. Mixed Mode: Here we consider the parameters ². Given these parameter values one finds that the oscillatory uniform state has an amplitude $\mathcal{H} = 1$ and destabilizes along the line $\Delta J_k = -1$. The standing waves solution has an amplitude $\mathcal{A}_{SW} = \sqrt{-\Delta J_k/8}$ (traveling waves are again unstable) which undergoes an oscillatory instability at $\Delta J_k = -2$. The mixed-mode solution is given by

$$(37a) \quad \mathcal{H} = \frac{8 + 2\Delta J_k(2 - \cos \phi - \sin \phi)}{8 - 2(2 - \cos \phi - \sin \phi)^2},$$

$$(37b) \quad \mathcal{A}_{SW} = \frac{\Delta J_k + (2 - \cos \phi - \sin \phi)}{8 - 2(2 - \cos \phi - \sin \phi)^2},$$

$$(37c) \quad \begin{aligned} 1 &= \Delta J_k(1 - 4 \cos \phi - 2 \sin \phi + 2 \sin \phi \cos \phi) \\ &\quad - 4 \cos \phi + 8 \cos \phi^2. \end{aligned}$$

It is easy to show that for $\Delta J_k \rightarrow -1$ the mixed mode amplitudes approach $(\mathcal{H}, \mathcal{A}_{SW}) = (1, 0)$ and the phase $\phi \rightarrow 0$. The mixed-mode solution thus bifurcates continuously from the oscillatory pure mode. Fig.12b shows the corresponding bifurcation diagram where solid and dotted lines are the analytical expressions for the solution branches and symbols are from numerical simulation of Eqs.28a -28c. As ΔJ_k increase from the left we see that the SW solution indeed undergoes an oscillatory instability at $\Delta J_k = -2$ leading to an oscillatory mixed-mode solution indicated by small circles (the maximum and minimum amplitude achieved on each cycle is shown). This oscillatory solution disappears in a saddle-node bifurcation, giving rise to a steady mixed-mode solution whose amplitude is given by Eq.37a- 37c. This steady mixed-mode solution bifurcates from the pure oscillatory mode at $\Delta J_k = -1$ as predicted.

4.1.3. Summary. The interaction between the oscillatory uniform state and waves may lead to mixed mode solutions or bistability. The OU state always destabilizes along the line $J_1 = J_0$, irrespective of parameter values or the choice of Φ or $J(x)$. This result from the weakly nonlinear analysis, agrees with numerical simulations of Eq.3 over the entire range of values of J_0 and J_1 used in the phase diagram, Fig.2 and appears to be exact. Depending on the value of J_2 , supercritical TW or supercritical SW will be stable near the codimension 2 point. In the case of TW, the slope of the stability line is one half the ratio of the cubic coefficient

² $\mu = -1$, $\Delta J_0 = 1$, $\alpha = -1$, $a = -8$, $\beta = 1$, $b = c = d = \omega = \Omega = 0$

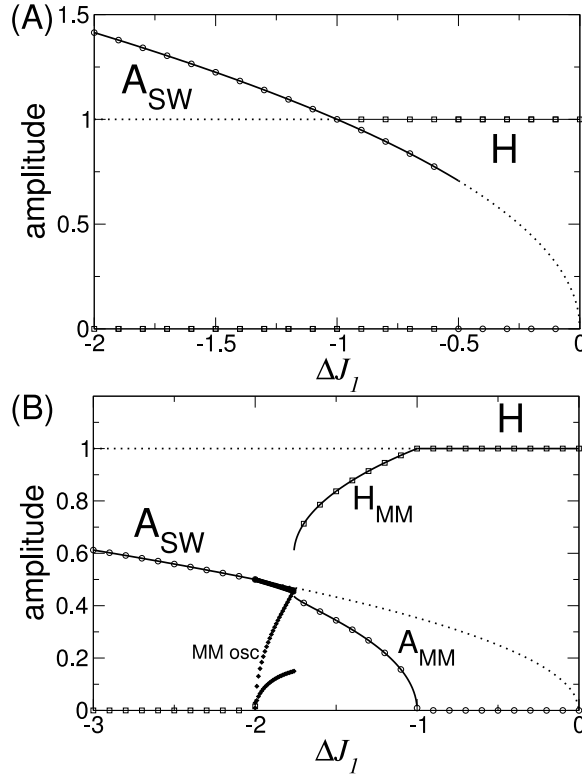


FIGURE 12. Two typical bifurcation diagrams for the case of harmonic resonance between small-amplitude oscillations and small-amplitude standing waves. A: Here oscillations and standing waves are bistable for $-1 < \Delta J_1 < -1/2$. $\Delta J_0 = -1$, $\alpha = -1$, $a = -1$, $b = c = d = \beta = \Omega = 0$, $\mu = -1$. B: Here the standing wave solution loses stability to an oscillatory mixed-mode solution at $\Delta J_1 = -2$. At $\Delta J_1 \sim -1.75$ a steady mixed-mode solution arises in a saddle-node bifurcation and continuously approaches the oscillatory pure-mode solution at $\Delta J_k = -1$. Parameters are $a = -8$, $\beta = 1$, $\alpha = -1$, $\mu = -1$, $b = c = d = \Omega = 0$. The phase ϕ of the mixed-mode solution is not shown.

of waves to that of oscillations. In the small delay limit this expression can be simplified to

$$(38) \quad \frac{a}{2\alpha} \sim \frac{\pi}{4} \frac{\left(\frac{(\Phi'')^2}{\Phi'} - \frac{\Phi'''}{2} \right)}{\left(\frac{(11\pi-4)(\Phi'')^2}{20\Phi'} - \frac{\pi\Phi'''}{4} \right)},$$

which depends only on shape of the transfer function Φ . For the parameter values used in the phase diagram Fig.2 this yields a line with slope close to one half. Thus TW and OU are expected to be bistable in the wedge between $\Delta J_1 = \Delta J_0/2$

and $\Delta J_1 = \Delta J_0$. In the case of SW, the slope of the stability line is a complicated function of the shape of Φ and the second Fourier coefficient J_2 . For the parameter values used in the phase diagram Fig.2 the slope is close to 0.6. Therefore the OU and SW states are bistable in the wedge between $\Delta J_1 = 0.6\Delta J_0$ and $\Delta J_1 = \Delta J_0$.

4.2. Hopf and Turing bifurcations. We consider the co-occurrence of two instabilities: a spatially homogeneous oscillation and a spatially inhomogeneous steady solution. This occurs when the zeroth spatial Fourier mode of the connectivity satisfies the relation, Eq.10b and the k_{th} spatial Fourier mode satisfies $J_k = 1/\Phi'$, while we assume that all other Fourier modes are sufficiently below their critical values to avoid additional instabilities. Without loss of generality we take $k = 1$ for the Turing instability.

We expand the parameters J_0 , J_1 , I and r as in Eqs. 13,14,15, and define the slow time Eq. 16. The linear solution consists of homogeneous, global oscillations and stationary, spatially periodic bumps with amplitudes which we allow to vary slowly in time, i.e. $r_1 = H(T)e^{i\omega t} + A(T)e^{ikx} + c.c.$. Carrying out a weakly nonlinear analysis to third order in ϵ leads to the coupled amplitude equations

$$\begin{aligned} \partial_T H &= (\mu + i\Omega)\Delta J_0 H + (\alpha + i\beta)|H|^2 H \\ (39a) \quad &\quad + (\kappa + i\Lambda)|A|^2 H, \end{aligned}$$

$$(39b) \quad \partial_T A = \bar{\eta}\Delta J_1 A + \Gamma|A|^2 A + \sigma|H|^2 A,$$

where $\mu + i\Omega$, $\alpha + i\beta$, $\bar{\eta}$, Γ , $\kappa + i\Lambda$ and σ are given by Eqs.51, 52, 18a, 18b, 64 and 65 respectively.

4.2.1. Solution types and their stability. Steady state solutions to Eqs.39a and 39b include pure mode OU, pure mode SB and mixed mode solutions (OU-SB). We look at the stability of the OU and SB solutions in turn for the general case and then look specifically at the case of small delay in Eq.3. Since the coupling in Eqs.39a -39b is only through the amplitudes we can simplify the equations by taking $(H, A) = (\mathcal{H}e^{i\theta}, \mathcal{A}e^{i\phi})$ which yields

$$(40a) \quad \dot{\mathcal{H}} = \mu\Delta J_0 \mathcal{H} + \alpha\mathcal{H}^3 + \kappa\mathcal{A}^2 \mathcal{H},$$

$$(40b) \quad \dot{\mathcal{A}} = \bar{\eta}\Delta J_1 \mathcal{A} + \Gamma\mathcal{A}^3 + \sigma\mathcal{H}^2 \mathcal{A}.$$

Uniform oscillations (OU): The oscillatory uniform solution has the form $(\bar{\mathcal{H}}, 0)$ where

$$\mathcal{H} = \sqrt{-\frac{\mu\Delta J_0}{\alpha}}.$$

The linear stability of this solution can be calculated with the ansatz

$$(\mathcal{H}, \mathcal{A}) = (\bar{\mathcal{H}} + \delta\mathcal{H}e^{\lambda t}, \delta\mathcal{A}e^{\lambda t}),$$

which yields the two eigenvalues

$$\lambda_H = -2\mu\Delta J_0,$$

$$\lambda_A = \eta\Delta J_1 + \frac{\mu\sigma}{\alpha}\Delta J_0.$$

If we assume a supercritical uniform oscillatory state then the first eigenvalue is always negative, while the second becomes positive along the line

$$(42) \quad \Delta J_1 = \frac{\mu\sigma}{\eta\alpha}\Delta J_0,$$

indicating the growth of a bump solution.

For Eq.3 with the parameters used to generate the phase diagram Fig.2, we find from Eq.42 that the OU state destabilizes along the line $\Delta J_1 \sim -0.026\Delta J_0$.

Stationary Bump (SB): The stationary bump solution has the form $(0, \bar{\mathcal{A}})$ where

$$\mathcal{A} = \sqrt{-\frac{\eta\Delta J_1}{\Gamma}}.$$

The linear stability of this solution can be calculated with the ansatz

$$(\mathcal{H}, \mathcal{A}) = (\delta\mathcal{H}e^{\lambda t}, \bar{\mathcal{A}} + \delta\mathcal{A}e^{\lambda t}),$$

which yields the two eigenvalues

$$\lambda_H = \mu\Delta J_0 - \frac{\eta\kappa}{\Gamma}\Delta J_1,$$

$$\lambda_A = -2\eta\Delta J_1.$$

If we assume a supercritical stationary bump state then the second eigenvalue is always negative, while the first becomes positive along the line

$$(44) \quad \Delta J_1 = \frac{\mu\Gamma}{\eta\kappa}\Delta J_0,$$

indicating the growth of uniform oscillations.

For Eq.3 with the parameters used to generate the phase diagram Fig.2, we find from Eq.44 that the SB state destabilizes along the line $\Delta J_1 \sim -0.144\Delta J_0$.

Mixed Mode (OU-SB): The mixed-mode solution satisfies the following matrix equation

$$\begin{pmatrix} \alpha & \kappa \\ \sigma & \Gamma \end{pmatrix} \begin{pmatrix} \mathcal{H}^2 \\ \mathcal{A}^2 \end{pmatrix} = - \begin{pmatrix} \mu\Delta J_0 \\ \eta\Delta J_1 \end{pmatrix},$$

which yields

$$\mathcal{H}^2 = \frac{-\mu\Gamma\Delta J_0 + \eta\kappa\Delta J_1}{\alpha\Gamma - \sigma\kappa},$$

$$\mathcal{A}^2 = \frac{\mu\sigma\Delta J_0 - \eta\alpha\Delta J_1}{\alpha\Gamma - \sigma\kappa}.$$

We do not study the stability of the mixed-mode solution here.

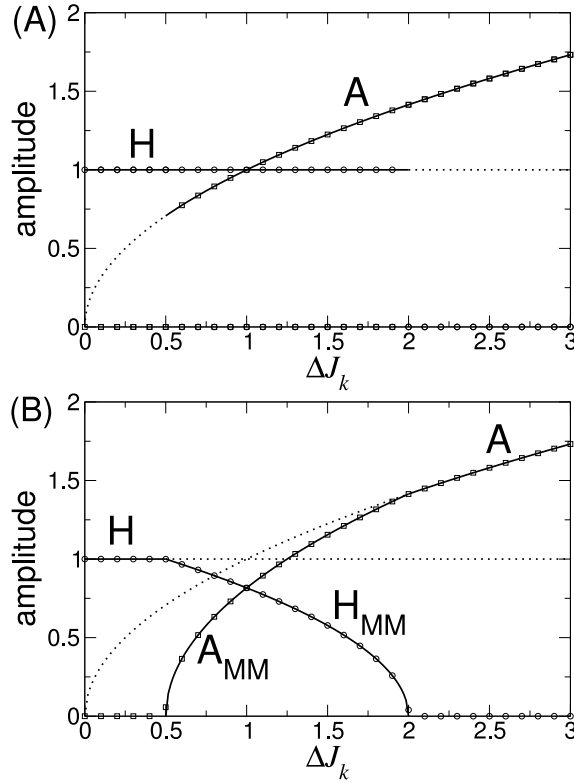


FIGURE 13. Typical bifurcation diagrams for the competition between bumps and global oscillations. $\mu = -1$, $\Delta J_0 = -1$, $\alpha = -1$, $\eta = 1$, $\Gamma = -1$. A: $\kappa = -2$, $\sigma = -2$. The limit cycle and bump solutions are bistable in the range $1/2 < \Delta J_1 < 2$. B: A mixed-mode solution is stable in the range $1/2 < \Delta J_1 < 2$. $\kappa = -0.5$, $\sigma = -0.5$. Symbols are from simulation of the amplitude equations Eqs.40a-40b while lines are the analytical expressions.

4.2.2. *A simple example.* We once again illustrate the scenarios of bistability and mixed-mode solutions with a simple example.

i. *Bistability:* Here we take the parameters³. In this case, the limit cycle has an amplitude $\mathcal{H} = 1$ and undergoes an instability at $\Delta J_1 = 2$. The bump solution has an amplitude $\mathcal{A} = \sqrt{\Delta J_1}$ and becomes unstable at $\Delta J_1 = 1/2$. The oscillatory and bump solutions are therefore bistable in the range $1/2 < \Delta J_1 < 2$. This is borne out in numerical simulations of Eqs.40a-40b, see Fig.13A. Symbols are from numerical simulation (circles:limit cycle, squares:bump), while lines are analytical solutions.

³ $\mu = \alpha = \Gamma = \Delta J_0 = -1$, $\sigma = \kappa = -2$

Bifurcations of Codimension 2	Solution types calculated	Instability boundaries
Hopf and Turing-Hopf	Oscillatory Uniform	$\Delta J_1 = \Delta J_0$
	Travelling Waves	$\Delta J_1 = a/(2\alpha)\Delta J_0$
	Standing Waves (oscillatory)	$\Delta J_1 = (a+c)/(4\alpha)\Delta J_0$
	Standing Waves (stationary)	$\Delta J_1 = \Psi\Delta J_0$
	Mixed-Mode	Not calculated
Hopf and Turing	Oscillatory Uniform	$\Delta J_1 = (\mu\sigma)/(\eta\alpha)\Delta J_0$
	Stationary Bump	$\Delta J_1 = (\mu\Gamma)/(\eta\kappa)\Delta J_0$
	Mixed-Mode (OU-SB)	Not calculated

TABLE 1. Some existing dynamical states that are present close to the codimension 2 bifurcations, and their corresponding instability boundaries Eqs. 29, 30, 33, 34, 42, 44 (except for the Mixed Mode solutions).

ii. Mixed-mode: Here we consider the parameters ⁴. In this case, the limit cycle has an amplitude $\mathcal{H} = 1$ and undergoes an instability at $\Delta J_1 = 1/2$. The bump solution has an amplitude $\mathcal{A} = \sqrt{\Delta J_1}$ and becomes unstable at $\Delta J_1 = 2$. The mixed-mode solution is stable in the range $1/2 < \Delta J_1 < 2$ and has amplitudes $\mathcal{H}_{MM} = 2\sqrt{(1 - \Delta J_1/2)/3}$ and $\mathcal{A} = 2\sqrt{(\Delta J_1 - 1/2)3}$. The corresponding bifurcation diagram is shown in Fig.13B where symbols are from simulation of Eqs.40a-40b and lines are the analytical results.

4.2.3. *Summary.* The interaction between the SB and OU states can lead to one of two scenarios. Either there is a region of bistability between bumps and oscillations, or there is a mixed-mode solution which, near the codimension 2 point at least, will consist of bumps whose amplitude oscillates in time, i.e. oscillating bumps (OB).

In the limit of small D the instability lines for the OU and SB states in the vicinity of the codimension 2 point are given by the equations

$$(46) \quad \Delta J_1 = -D \frac{\left(\frac{(\Phi'')^2}{\Phi'} - \Phi''' \right)}{\left(\frac{(11\pi-4)}{20} \frac{(\Phi'')^2}{\Phi'} - \pi \frac{\Phi'''}{4} \right)} \Delta J_0,$$

$$(47) \quad \Delta J_1 = -\frac{2}{\pi} D \frac{\left(\frac{(\Phi'')^2}{\Phi'} - \frac{\Phi'''}{2} - \frac{J_2(\Phi'')^2}{2(1-J_2\Phi')} \right)}{\left(\frac{(\Phi'')^2}{\Phi'} - \Phi''' \right)} \Delta J_0.$$

respectively. The slope of both of the stability lines is proportional to D , indicating that in the small D limit any region of bistability or mixed mode solution

⁴ $\mu = \alpha = \Gamma = \Delta J_0 = -1$, $\sigma = \kappa = -1/2$

will be limited to a narrow wedge close to the J_0 axis. Which scenario will be observed (bistability or mixed-mode) depends on the particular choice of Φ' and the value of the second spatial Fourier mode of the connectivity J_2 . For the parameters values used to generate the phase diagram Fig.2 the slopes are ~ -0.026 and ~ -0.144 for the OU and SB stability lines respectively, indicating a mixed mode solution.

5. CONCLUSIONS

In this paper we have studied the nature and stability of solutions arising via a primary instability of a fixed point in a rate equation with fixed delay, Eq.3. The four possible primary instabilities are: i. - a steady rate instability for sufficiently strong recurrent excitation which leads to a high activity state, ii. - a Turing instability for Mexican hat connectivity which leads to stationary bumps, iii. - a Hopf instability for sufficiently strong recurrent inhibition which leads to an oscillatory uniform state, iv. - a Turing-Hopf instability for strong local inhibition and longer-range excitation (inverted Mexican hat) which leads to waves. We have focused on the oscillatory instabilities which arise only for a non-zero delay, i.e. they are delay-driven. The instability mechanism due to the delay can be understood intuitively. We need only assume that the coupling in the system is predominantly inhibitory and that there is a fixed delay D in the interactions between neurons. In this case, if the state of the system is perturbed at a time t , causing an increase in activity, then this increase in activity will generate a corresponding decrease in activity after a time $\sim D$. This decrease in activity leads to an increase in activity again after a time $\sim D$. In this way oscillations can emerge. This argument does not tell us how strong the inhibition must be to maintain oscillations, and this will depend on the details of the system. Additionally it is clear that this mechanism is only valid for inhibitory and not excitatory feedback.

An equation of the form Eq.3 with a threshold linear transfer function and cosine connectivity was studied already in [Roxin et al.(2005)], [Roxin et al.(2006)]. The simple choice of transfer function and connectivity allowed the authors to construct a phase diagram of dynamical states to a large extent analytically. Many of the dynamical states predicted by this analysis were subsequently confirmed through simulations of recurrently coupled spiking neurons [Roxin et al.(2005)], [Roxin et al.(2006)]. One discrepancy concerned the Turing-Hopf instability which in the rate equation lead to traveling waves (TW) and in the network simulations to standing waves (SW). Here we have shown that including a transfer function with an expansive nonlinearity in the rate equation correctly predicts a SW state given a simple cosine connectivity. We additionally predicted that a TW state should be seen once a sufficiently large and negative second spatial Fourier mode was included in the connectivity. This was borne out in network simulations of Hodgkin-Huxley neurons, see Fig.3.3.1. This explains

the discrepancy in the previous work but, in fact, makes the much more general point that the specific form of the transfer function (or fI curve) and the synaptic connectivity may be important in determining the dynamical state observed during spontaneous activity in neuronal networks. We have shown that the same principle holds true regarding the nature of dynamical states near a bifurcation point, e.g. whether or not the solution is subcritical or supercritical or which type of solution will be observed if several exist and must compete as is the case with SW and TW states.

In general the nature of a dynamical state in Eq.3 near one of the primary instability lines depends on a complicated combination of the first three derivatives of the transfer function at the fixed point and the first three spatial Fourier coefficients of the synaptic connectivity. We have derived these expressions and their asymptotic approximations in the limit of small delay. Despite the complexity of these expressions we have tried to answer two specific qualitative questions: 1 - are delay-driven oscillations in general supercritical or subcritical?, 2 - given realistic patterns of synaptic connectivity which is the most likely wave state, TW or SW? The nature of the oscillatory uniform state depends on the balance of the first three derivatives of the transfer function. We find that whether the transfer function represents the fraction of active neurons [Wilson and Cowan(1972)] or the fI curve of a cortical cell driven by noisy inputs [Miller and Troyer(2002)], [Hansel and van Vreeswijk(2002)], the oscillations are likely to be supercritical. This agrees with numerical simulations of Hodgkin-Huxley neurons (not shown here) as well as with the amplitude equation derived analytically for a network of integrate-and-fire neurons [Brunel and Hakim(1999)]. We also find that for patterns of synaptic connectivity which decay in space, e.g. Gaussian, the TW state is favored for small delay. The reason for this is that the competition between SW and TW in the small delay limit depends strongly on the sign and strength of J_2 , the second spatial Fourier mode of the connectivity, see Eq.25. At the Turing-Hopf bifurcation point, J_1 , the bifurcation parameter, is equal to its critical value which is large and negative. The value of J_2 is constrained by J_1 to relatively large and negative values as well as long as the connectivity is narrow enough compared to the width of the system, i.e. it should go to zero at the boundaries, in this case at $-\pi$ and π , see Fig.3.3.1. Large and negative values of J_2 favor the TW state by Eq.25. Both of these findings are dependent on the parameter D in Eq.3 being small. As argued in the introduction this seems reasonable since D represents the ratio of the fixed delay in interactions to the membrane time constant which are on the order of 1ms and 10ms respectively.

Finally, we have tried to emphasize the importance of fixed delays in shaping the dynamics described by Eq.3 and by extension in networks of spiking neurons. Nonetheless both fixed and conduction delays are present in neuronal systems and are roughly of the same order of magnitude in a small patch of cortex of $\sim 1\text{mm}$ in extent. It remains to be studied how these delays interact to shape patterns of spontaneous activity.

APPENDIX A. AMPLITUDE EQUATIONS

In this appendix we outline the calculation of the amplitude equations which describe the slow temporal evolution of the various instabilities near their respective bifurcations.

A.1. General framework for the weakly nonlinear calculation: Codimension 1 bifurcations. Here we briefly describe the general framework for the weakly nonlinear calculation for the Turing, Hopf and Turing-Hopf bifurcations. We use a multiple-scales approach which takes advantage of the fact there is a near-zero eigenvalue in the vicinity of a bifurcation which is responsible for the slow temporal evolution of the critical eigenmode. This is a standard method, see e.g. [Holmes(1995)].

For simplicity we first rewrite Eq.3 as

$$(48) \quad \dot{r} = -r + \Phi(\langle J_r \rangle + I),$$

where $\langle fg \rangle \equiv \frac{1}{2\pi} \int_{-\pi}^{\pi} dy f(y-x)g(y, t-D)$. We study the stability of the steady state solution $R = \Phi(J_0 R + I)$, where $J(x) = J_0 + 2 \sum_{n=1}^{\infty} J_n \cos nx$. We expand the rates, the connectivity and the input current as

$$\begin{aligned} r(x, t) &= R + \epsilon r_1(x, t, T) + \epsilon r_2(x, t, T) + \dots, \\ J(x) &= \bar{J}(x) + \epsilon^2 \Delta J(x), \\ I &= \bar{I} + \epsilon^2 \Delta I, \end{aligned}$$

where the small parameter ϵ is defined by the distance from the critical value of the connectivity. Plugging these expansions into Eq.48 yields

$$(\mathcal{L} + \epsilon^2 \mathcal{L}_2)(\epsilon r_1 + \epsilon^2 r_2 + \dots) = \epsilon^2 N_2(r_1) + \epsilon^3 N_3(r_1, r_2),$$

where

$$\begin{aligned} \mathcal{L}r &= \partial_t r + r - \langle \bar{J}r \rangle, \\ \mathcal{L}_2 r &= \partial_T \langle \bar{J}r \rangle - \langle \Delta J r \rangle, \\ N_2 &= \frac{\Phi''}{2} \langle \bar{J}r_1 \rangle^2, \\ N_3 &= \Phi'' \langle \bar{J}r_1 \rangle \langle \bar{J}r_2 \rangle + \frac{\Phi'''}{6} \langle \bar{J}r_1 \rangle^3. \end{aligned}$$

We now collect terms by order in ϵ . At first order we have

$$\vartheta(\epsilon) : \quad \mathcal{L}r_1 = 0.$$

This equation gives the linear dispersion relation Eq.8. The values of the connectivity and input current for which it is satisfied are $J(x) = \bar{J}(x)$ and $I = \bar{I}$.

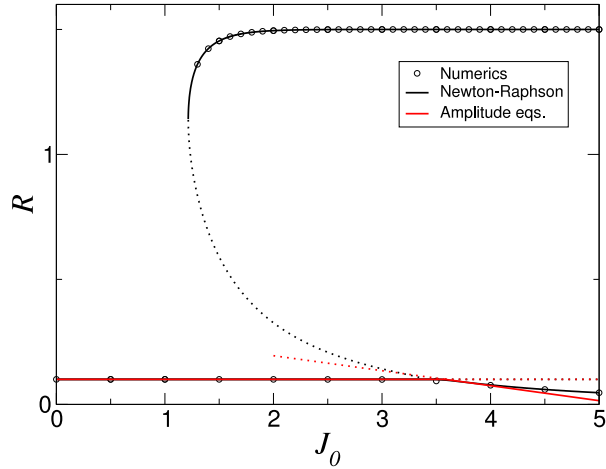


FIGURE 14. (Color online) Bifurcation diagram for the steady instability. Open circles: numerical simulation of Eq.3. Red Lines: amplitude equation solution from Eq.50. Black lines: steady-state solution of Eq.3 using a Newton-Raphson solver. Solid lines indicate stable solutions and dotted lines unstable ones. $\Phi(x) = \frac{\alpha}{1+e^{-\beta x}}$ where $\alpha = 1.5$ and $\beta = 3$. $J(x) = J_0 + J_1 \cos x$ where $J_1 = 0$. The input current I is varied so as to keep the uniform stationary solution fixed at $R = 0.1$.

At second order we obtain

$$\vartheta(\epsilon^2) : \quad \mathcal{L}r_2 = N_2(r_1).$$

The second order solution r_2 is the particular solution of this linear differential equation. And finally, at third order

$$\vartheta(\epsilon^3) : \quad \mathcal{L}r_3 = N_3(r_1, r_2) - \mathcal{L}_2 r_1.$$

At this order secular terms arise which have the same temporal and/or spatial frequency as the linear solution. In order for the above equation to have a solution, these terms must therefore be eliminated, yielding the desired amplitude equation for the instability.

A.1.1. Steady Bifurcation: $\omega = 0$, $k = 0$. For completeness we include here the derivation of the amplitude equation for the transcritical bifurcation.

The 0^{th} spatial Fourier mode of the connectivity is given by the critical value $\bar{J}_0 = \frac{1}{\Phi'}$, while we assume that all other Fourier modes are sufficiently below their

critical values to avoid additional instabilities. We expand

$$(49) \quad \begin{aligned} J_0 &= \bar{J}_0 + \epsilon \Delta J_0, \\ I &= \bar{I} + \epsilon \Delta I, \\ r &= R + \epsilon r_1 + \epsilon^2 r_2 + \dots, \end{aligned}$$

where the small parameter ϵ is defined by Eq.49. We define the slow time $T = \epsilon t$. The linear solution is a spatially homogeneous amplitude which we allow to vary slowly in time, i.e. $r_1 = A(T)$. Carrying out a weakly nonlinear analysis to second order in ϵ leads to the normal form for a transcritical bifurcation given by

$$(50) \quad \begin{aligned} \partial_T A &= \eta \Delta J_0 A + \gamma A^2, \\ \eta &= \frac{\Phi'}{1+D}, \\ \gamma &= \frac{\Phi''}{2(1+D)} \bar{J}_0^2. \end{aligned}$$

A.1.2. *Turing bifurcation.* $\vartheta(\epsilon)$: The solution to the linear equation is spatially periodic with slowly varying amplitude A ,

$$r_1 = A(T) e^{ikx} + c.c.$$

$\vartheta(\epsilon^2)$: The nonlinear forcing and resulting second order solution are

$$\begin{aligned} N_2 &= \Phi'' J_k^2 (A^2 e^{2ikx} + c.c. + 2|A|^2)/2, \\ r_2 &= r_{22} e^{2ikx} + c.c. + r_{20}, \\ r_{22} &= \frac{\Phi'' J_k^2}{2(1 - J_{2k} \Phi')} A^2, \\ r_{20} &= \frac{\Phi'' J_k^2}{1 - J_0 \Phi'} |A|^2. \end{aligned}$$

$\vartheta(\epsilon^3)$: The nonlinear forcing at cubic order is

$$\begin{aligned} N_3 &= (\Phi'' J_k J_0 A r_{20} + \Phi'' J_k J_{2k} \bar{A} r_{22} \\ &\quad + \Phi''' J_k^3 |A|^2 A/2) e^{ikx} + c.c. + \dots \end{aligned}$$

Eliminating all terms of periodicity e^{ikx} at this order yields the amplitude equation, Eq.17.

$$\partial_T A = \eta \Delta J_k A + \Gamma |A|^2 A,$$

with the coefficients

$$\eta = \frac{\Phi'}{1+D},$$

$$\Gamma = \frac{\bar{J}_k^3}{1+D} \left(\frac{J_0(\Phi'')^2}{1-J_0\Phi'} + \frac{J_{2k}(\Phi'')^2}{2(1-J_{2k}\Phi')} + \frac{\Phi'''}{2} \right).$$

A.1.3. *Hopf bifurcation.* $\vartheta(\epsilon)$: The solution to the linear equation is a time periodic function with slowly varying amplitude H

$$r_1 = H(T)e^{i\omega t} + c.c.$$

$\vartheta(\epsilon^2)$: The nonlinear forcing and resulting second order solution are

$$N_2 = \Phi'' J_0^2 (H^2 e^{2i\omega(t-D)} + c.c. + 2|H|^2)/2,$$

$$r_2 = r_{22} e^{2i\omega t} + c.c. + r_{20},$$

$$r_{22} = \frac{\Phi'' J_0^2}{2(2i\omega + 1 - \Phi' J_0 e^{-2i\omega D})} e^{-2i\omega D} H^2,$$

$$r_{20} = \frac{\Phi'' J_0^2}{1 - J_0 \Phi'} |H|^2.$$

$\vartheta(\epsilon^3)$: The nonlinear forcing at cubic order is

$$N_3 = (\Phi'' J_0^2 H r_{20} + \Phi'' J_0^2 \bar{H} r_{22} + \Phi''' J_0^3 |A|^2 A/2) e^{i\omega(t-D)} + c.c. + \dots$$

Eliminating all terms of periodicity $e^{i\omega t}$ at this order yields the amplitude equation, Eq.19.

$$\partial_T H = (\mu + i\Omega) \Delta J_0 H + (\alpha + i\beta) |H|^2 H,$$

with the coefficients

$$(51) \quad \mu + i\Omega = \frac{\Phi' e^{-i\omega D}}{1 + D(1 + i\omega)},$$

$$(52) \quad \alpha + i\beta = \frac{e^{-i\omega D}}{1 + D(1 + i\omega)} \times$$

$$\left(\frac{\bar{J}_0^4 (\Phi'')^2}{1 - \Phi' \bar{J}_0} + \frac{\bar{J}_0^4 (\Phi'')^2 e^{-2i\omega D}}{2(2i\omega + 1 - \Phi' \bar{J}_0 e^{-2i\omega D})} + \frac{\bar{J}_0^3 \Phi'''}{2} \right).$$

A.1.4. *Turing-Hopf bifurcation.* $\vartheta(\epsilon)$: The solution to the linear equation are two sets of periodic waves, one left-traveling with slowly varying amplitude A and the other right-traveling with slowly varying amplitude B

$$\begin{aligned} r_1 &= A(T)e^{i\omega t+ikx} + B(T)e^{-i\omega t+ikx} + c.c. \\ &= A(T)e^\psi + B(T)e^\phi + c.c. \end{aligned}$$

$\vartheta(\epsilon^2)$: The nonlinear forcing and resulting second order solution are

$$\begin{aligned} N_2 &= \Phi'' J_k^2 (A^2 e^{2\psi - 2i\omega D} + 2ABe^{\psi+\phi} + 2A\bar{B}e^{\psi+\bar{\phi}-2i\omega D} + B^2 e^{2\phi+2i\omega D} + c.c. \\ &\quad + 2(|A|^2 + |B|^2))/2, \\ r_2 &= r_{2\psi} e^{2\psi} + r_{\psi\phi} e^{\psi+\phi} + r_{\psi\bar{\phi}} e^{\psi+\bar{\phi}} + r_{2\phi} e^{2\phi} + c.c. + r_{20}, \\ r_{2\psi} &= \frac{\Phi'' J_k^2}{2(2i\omega + 1 - \Phi' J_{2k} e^{-2i\omega D})} e^{-2i\omega D} A^2, \\ r_{\psi\phi} &= \frac{\Phi'' J_k^2}{1 - \Phi' J_{2k}} AB, \\ r_{\psi\bar{\phi}} &= \frac{\Phi'' J_k^2}{2i\omega + 1 - J_0 \Phi' e^{-2i\omega D}} e^{-2i\omega D} A\bar{B}, \\ r_{2\phi} &= \frac{\Phi'' J_k^2}{2(-2i\omega D + 1 - J_{2k} \Phi' e^{2i\omega D})} e^{2i\omega D} B^2, \\ r_{20} &= \frac{\Phi'' J_k^2 (|A|^2 + |B|^2)}{1 - J_0 \Phi'}. \end{aligned}$$

$\vartheta(\epsilon^3)$: The nonlinear forcing at cubic order is

$$(53) \quad N_3 = \left(\Phi'' J_k J_0 A r_{20} + \Phi'' J_k J_{2k} \bar{A} r_{2\psi} + \Phi'' J_k J_0 B r_{\psi\bar{\phi}} + \Phi'' J_k J_{2k} \bar{B} r_{\psi\phi} \right. \\ \left. + \Phi''' |A|^2 A / 2 + \Phi''' |B|^2 A \right) e^{\psi-i\omega D}$$

$$(54) \quad \begin{aligned} &+ \left(\Phi'' J_k J_0 A \bar{r}_{\psi\bar{\phi}} + \Phi'' J_k J_{2k} \bar{A} r_{\psi\phi} + \Phi'' J_k J_0 B r_{20} + \Phi'' J_k J_{2k} \bar{B} r_{2\phi} \right. \\ &\quad \left. + \Phi''' |B|^2 B / 2 + \Phi''' |A|^2 B \right) e^{\phi+i\omega D} \\ &+ \dots \end{aligned}$$

Eliminating all terms with dependencies $e^{i\psi}$ and $e^{i\phi}$ yields the two coupled amplitude equations Eqs.22a and 22b.

$$\begin{aligned} \partial_T A &= (\mu + i\Omega) \Delta J_k A + (a + ib)|A|^2 A + (c + id)|B|^2 A, \\ \partial_T B &= (\mu - i\Omega) \Delta J_k B + (a - ib)|B|^2 B + (c - id)|A|^2 B, \end{aligned}$$

with the coefficients

$$(55) \quad a + ib = \frac{\bar{J}_k^3 e^{-i\omega D}}{1 + D\Phi' \bar{J}_k e^{-i\omega D}} \left(\frac{J_0(\Phi'')^2}{1 - \Phi' J_0} + \frac{J_{2k}(\Phi'')^2 e^{-2i\omega D}}{2(2i\omega + 1 - \Phi' J_{2k} e^{-2i\omega D})} + \frac{\Phi'''}{2} \right),$$

$$(56) \quad c + id = \frac{\bar{J}_k^3 e^{-i\omega D}}{1 + D\Phi' \bar{J}_k e^{-i\omega D}} \left(\frac{J_0(\Phi'')^2}{1 - \Phi' J_0} + \frac{J_0(\Phi'')^2 e^{-2i\omega D}}{2i\omega + 1 - \Phi' J_0 e^{-2i\omega D}} + \frac{J_{2k}(\Phi'')^2}{1 - \Phi' J_{2k}} + \Phi''' \right).$$

A.2. Codimension 2 bifurcations.

A.2.1. *Double zero eigenvalue: Hopf, Turing-Hopf.* $\vartheta(\epsilon)$: The solution to the linear equation are periodic oscillations and traveling waves

$$\begin{aligned} r_1 &= H(T) + e^{i\omega t} + A(T)e^{i\omega t+ikx} + B(T)e^{-i\omega t+ikx} + c.c. \\ &= H(T)e^{i\omega t} + A(T)e^\psi + B(T)e^\phi + c.c. \end{aligned}$$

$\vartheta(\epsilon^2)$: The nonlinear forcing and resulting second order solution are

$$\begin{aligned} N_2 &= \Phi'' J_0^2 (H^2 e^{2i\omega(t-D)} + c.c. + 2|H|^2)/2 + \Phi'' J_k^2 (A^2 e^{2\psi-2i\omega D} + 2ABe^{\psi+\phi} \\ &\quad + 2A\bar{B}e^{\psi+\bar{\phi}-2i\omega D} + B^2 e^{2\phi+2i\omega D} + c.c. + 2(|A|^2 + |B|^2))/2 \\ &\quad + \Phi'' J_0 J_k (HAe^{2i\omega(t-D)+ix} + \bar{H}Be^{-2i\omega(t-D)+ix} + \bar{H}Ae^{ix} + HBe^{ix} + c.c.), \\ r_2 &= r_{22}e^{2i\omega t} + r_{2\psi}e^{2\psi} + r_{\psi\phi}e^{\psi+\phi} + r_{\psi\bar{\phi}}e^{\psi+\bar{\phi}} + r_{2\phi}e^{2\phi} + r_{HA}e^{2i\omega t+ix} \\ &\quad + r_{\bar{H}B}e^{-2i\omega t+ix} + r_{\bar{H}A}e^{ix} + r_{HB}e^{ix} + c.c. + r_{20}, \\ r_{HA} &= \frac{\Phi'' J_0 J_k}{2i\omega + 1 - \Phi' J_k e^{-2i\omega D}} e^{-2i\omega D} HA, \\ r_{\bar{H}B} &= \frac{\Phi'' J_0 J_k}{-2i\omega + 1 - \Phi' J_k e^{2i\omega D}} e^{2i\omega D} \bar{H}B, \\ r_{\bar{H}A} &= \frac{\Phi'' J_0 J_k}{1 - \Phi' J_k} \bar{H}A, \\ r_{HB} &= \frac{\Phi'' J_0 J_k}{1 - \Phi' J_k} HB, \\ r_{20} &= \frac{\Phi'' (J_0^2 |H|^2 + J_k^2 |A|^2 + J_k^2 |B|^2)}{1 - J_0 \Phi'}. \end{aligned}$$

$\vartheta(\epsilon^3)$: The nonlinear forcing at cubic order is

$$\begin{aligned} N_3 = & (\Phi'' J_0^2 H r_{20} + \Phi'' J_0^2 \bar{H} r_{22} + \Phi''' J_0^3 |H|^2 H / 2 + \Phi'' J_k^2 (A \bar{r}_{\bar{H}A} + \bar{A} r_{HA} + \bar{B} r_{\bar{H}A} \\ & + B \bar{r}_{\bar{H}B} + A \bar{r}_{HB} + \bar{B} r_{HB})) e^{i\omega(t-D)} \\ & + (\Phi'' J_k J_0 A r_{20} + \Phi'' J_k J_{2k} \bar{A} r_{2\psi} + \Phi'' J_k J_0 B r_{\psi\bar{\phi}} + \Phi'' J_k J_{2k} \bar{B} r_{\psi\phi} \\ & + \Phi''' |A|^2 A / 2 + \Phi''' |B|^2 A + \Phi'' J_0 J_k (H r_{\bar{H}A} + H r_{HB} + \bar{H} r_{HA})) e^{\psi - i\omega D} \\ & + (\Phi'' J_k J_0 A \bar{r}_{\psi\bar{\phi}} + \Phi'' J_k J_{2k} \bar{A} r_{\psi\phi} + \Phi'' J_k J_0 B r_{20} + \Phi'' J_k J_{2k} \bar{B} r_{2\phi} \\ & + \Phi''' |B|^2 B / 2 + \Phi''' |A|^2 B + \Phi'' J_0 J_k (H r_{\bar{H}B} + \bar{H} r_{\bar{H}A} + \bar{H} r_{HB})) e^{\phi + i\omega D}) \\ & + \dots \end{aligned}$$

Eliminating terms with dependencies $e^{i\omega t}$, $e^{i\psi}$ and $e^{i\phi}$ yields the three coupled amplitude equations, Eqs.28a-28c.

$$\partial_T H = (\mu + i\Omega) \Delta J_0 H + 2(\alpha + i\beta) \left[\left(\frac{|H|^2}{2} + |A|^2 + |B|^2 \right) H + \bar{H} A \bar{B} \right],$$

$$\partial_T A = (\mu + i\Omega) \Delta J_k A + (a + ib) |A|^2 A + (c + id) |B|^2 A + (\alpha + i\beta) [2|H|^2 A + H^2 B],$$

$$\partial_T B = (\mu - i\Omega) \Delta J_k B + (a - ib) |B|^2 B + (c - id) |A|^2 B + (\alpha - i\beta) [2|H|^2 B + \bar{H}^2 A],$$

where $\alpha + i\beta$, $a + ib$ and $c + id$ are given by Eqs.52, 55 and 56, respectively.

In the small delay limit ($D \rightarrow 0$) we can use the asymptotic values given by Eqs.12 to obtain, to leading order,

$$(57) \quad a + ib = -\frac{\chi(\frac{\pi}{2} + i)}{(D\Phi)^3} \left(\frac{(\Phi'')^2}{\Phi'} - \frac{\Phi'''}{2} \right),$$

$$\begin{aligned} (58) \quad c + id = & -\frac{\chi}{(D\Phi)^3} \left(\frac{(\Phi'')^2}{\Phi'} \frac{(3\pi - 2)}{5} - \frac{\pi}{2} \frac{J_{2k}(\Phi'')^2}{1 - \Phi' J_{2k}} - \frac{\pi \Phi'''}{2} \right. \\ & \left. + i \left[\frac{(\Phi'')^2}{\Phi'} \frac{(6 + \pi)}{5} - \frac{J_{2k}(\Phi'')^2}{1 - \Phi' J_{2k}} - \Phi'''' \right] \right). \end{aligned}$$

where $\chi \equiv \pi^3 / (8(1 + \frac{\pi^2}{4}))$ and $\alpha + i\beta$ is given by Eq.20b.

Solutions and their stability

Oscillatory uniform OU:

This solution can be expressed as $(H, A, B) = (\mathcal{H} e^{i\omega t}, 0, 0)$, where

$$\begin{aligned} \mathcal{H} &= \sqrt{\frac{-\mu \Delta J_0}{\alpha}}, \\ \omega &= \left(\Omega - \frac{\beta \mu}{\alpha} \right) \Delta J_0. \end{aligned}$$

The stability of this solution can be studied with the ansatz

$$(H, A, B) = (\mathcal{H}e^{i\omega t}(1 + \delta H_+ e^{\lambda t} + \delta \bar{H}_- e^{\bar{\lambda} t}), \\ e^{i\omega t}(\delta A_+ e^{\lambda t} + \delta \bar{A}_- e^{\bar{\lambda} t}), \\ e^{-i\omega t}(\delta B_+ e^{\lambda t} + \delta \bar{B}_- e^{\bar{\lambda} t})),$$

which leads to three pairs of coupled linear equations which determine the six eigenvalues λ . The first pair is restricted to the linear subspace of the small amplitude limit cycle and results in the standard stability problem which yields one stable eigenvalue $\lambda = -\mu\Delta J_0$ and one zero eigenvalue corresponding to a shift in the phase of the oscillation. The other two pairs, which span the subspaces of $(\delta A_+, \delta B_+)$ and $(\delta A_-, \delta B_-)$ respectively, give

$$\begin{pmatrix} \lambda - \mu\Delta J_1 - 2\alpha\mathcal{H}^2 + i(\Omega(\Delta J_0 - \Delta J_1) - \beta\mathcal{H}^2) & -(\alpha + i\beta)\mathcal{H}^2 \\ -(\alpha - i\beta)\mathcal{H}^2 & \lambda - \mu\Delta J_1 - 2\alpha\mathcal{H}^2 - i(\Omega(\Delta J_0 - \Delta J_1) - \beta\mathcal{H}^2) \end{pmatrix} \begin{pmatrix} \delta A_+ \\ \delta B_+ \end{pmatrix} = 0,$$

and the complex conjugate matrix spanning $(\delta A_-, \delta B_-)$. Setting the determinant equal to zero yields the characteristic equation

$$\lambda^2 - 2\lambda(\Delta J_1 - 2\Delta J_0)\mu + \mu^2(\Delta J_1 - 4\Delta J_1\Delta J_0 + 3\Delta J_0) \\ + \Omega^2(\Delta J_1 - \Delta J_0)^2 - 2\frac{\beta}{\alpha}\mu\Omega\Delta J_0(\Delta J_1 - \Delta J_0) = 0.$$

There is an oscillatory instability for $\Delta J_1 = 2\Delta J_0$ while a steady instability occurs for $\Delta J_1 = \Delta J_0$. The steady instability therefore always precedes the oscillatory one.

Traveling waves TW:

This solution can be expressed as $(H, A, B) = (0, \mathcal{A}_{TW}e^{i\omega t}, 0)$, where

$$\mathcal{A}_{TW} = \sqrt{\frac{-\mu\Delta J_1}{a}}, \\ \omega = \left(\Omega - \frac{b\mu}{a}\right)\Delta J_1.$$

The stability of this solution can be studied with the ansatz

$$(H, A, B) = (e^{i\omega t}(\delta H_+ e^{\lambda t} + \delta \bar{H}_- e^{\bar{\lambda} t}), \\ \mathcal{A}_{TW}e^{i\omega t}(1 + \delta A_+ e^{\lambda t} + \delta \bar{A}_- e^{\bar{\lambda} t}), \\ e^{-i\omega t}(\delta B_+ e^{\lambda t} + \delta \bar{B}_- e^{\bar{\lambda} t})),$$

which results in four coupled linear equations corresponding to the stability problem for TW in the competition between SW and TW (see section D, Turing-Hopf Bifurcation). Here we assume that the TW solution is supercritical and stable.

We then turn our attention to the remaining two linear equations which describe the growth of the oscillatory uniform mode. These equations are uncoupled and yield the complex conjugate eigenvalues

$$\lambda = -\mu \left(2\frac{\alpha}{a} \Delta J_1 - \Delta J_0 \right) \pm i \left(\Omega \left(1 - \frac{a}{2\alpha} \right) + (b - 2\beta) \frac{\mu}{2\alpha} \right) \Delta J_0,$$

from which it is easy to see that an instability occurs for $\Delta J_1 = \frac{a}{2\alpha} \Delta J_0$. This instability will generically occur with non-zero frequency.

Standing waves SW:

This solution can be expressed as $(H, A, B) = (0, \mathcal{A}_{SW} e^{i\omega t}, \mathcal{A}_{SW} e^{-i\omega t})$, where \mathcal{A}_{SW} and ω are given by equations (Eqs.31 and 32)

$$\begin{aligned} \mathcal{A}_{SW} &= \sqrt{\frac{-\mu \Delta J_1}{(a+c)}}, \\ \omega &= \left(\Omega - \frac{(b+d)}{(a+c)} \mu \right) \Delta J_1. \end{aligned}$$

The stability of this solution can be studied with the ansatz

$$\begin{aligned} (H, A, B) &= (e^{i\omega t} (\delta H_+ e^{\lambda t} + \delta \bar{H}_- e^{\bar{\lambda} t}), \\ &\quad \mathcal{A}_{SW} e^{i\omega t} (1 + \delta A_+ e^{\lambda t} + \delta \bar{A}_- e^{\bar{\lambda} t}), \\ &\quad \mathcal{A}_{SW} e^{-i\omega t} (1 + (\delta B_+ e^{\lambda t} + \delta \bar{B}_- e^{\bar{\lambda} t}))). \end{aligned}$$

This ansatz results in four coupled equations for the stability of SW in the competition between SW and TW. Here we assume that the SW solution is supercritical and stable. The remaining two equations describe the growth of the oscillatory uniform mode.

$$(59) \quad \begin{pmatrix} \lambda + i\omega - (\mu + i\Omega) \Delta J_0 - 4\mathcal{A}_{SW}(\alpha + i\beta) & -2\mathcal{A}_{SW}(\alpha + i\beta) \\ -2\mathcal{A}_{SW}(\alpha - i\beta) & \lambda - i\omega - (\mu - i\Omega) \Delta J_0 - 4\mathcal{A}_{SW}(\alpha - i\beta) \end{pmatrix} \begin{pmatrix} \delta H_+ \\ \delta \bar{H}_- \end{pmatrix} = 0.$$

Setting the determinant to zero yields the characteristic equation for the eigenvalues

$$\begin{aligned} (60) \quad & \lambda^2 - 2\mu\lambda \left(\Delta J_0 - 4\frac{\alpha}{(a+c)} \Delta J_1 \right) + \mu^2 \left(\Delta J_0 - 4\frac{\alpha}{(a+c)} \Delta J_1 \right)^2 \\ & + \left(\Delta J_1 \left(\Omega - \frac{(b+d)}{(a+c)} \mu + \frac{4\beta}{(a+c)} \mu \right) - \Omega \Delta J_0 \right)^2 \\ & - \frac{4}{(a+c)^2} \mu^2 \Delta J_1^2 (\alpha^2 + \beta^2) = 0. \end{aligned}$$

The conditions for oscillatory and steady instabilities, Eqs.33 and 34, are found by setting λ equal to $i\bar{\omega}$ and 0 respectively.

Mixed Mode:

Mixed mode solutions are found by applying the ansatz Eq.36 to Eqs.28a-28c. This gives

$$(61) \quad \begin{aligned} \dot{\mathcal{H}} &= \mu\Delta J_0\mathcal{H} + \alpha(\mathcal{H}^2 + 2\mathcal{A}^2 + 2\mathcal{B}^2)\mathcal{H} + 2\mathcal{H}\mathcal{A}\mathcal{B}(\alpha \cos \phi - \beta \sin \phi), \\ \dot{\mathcal{A}} &= \mu\Delta J_1\mathcal{A} + a\mathcal{A}^3 + c\mathcal{B}^2\mathcal{A} + 2\alpha\mathcal{H}^2\mathcal{A} + \mathcal{H}^2\mathcal{B}(\alpha \cos \phi + \beta \sin \phi), \\ \dot{\mathcal{B}} &= \mu\Delta J_1\mathcal{B} + a\mathcal{B}^3 + c\mathcal{A}^2\mathcal{B} + 2\alpha\mathcal{H}^2\mathcal{B} + \mathcal{H}^2\mathcal{A}(\alpha \cos \phi + \beta \sin \phi), \\ \dot{\phi} &= 2\Omega(\Delta J_1 - \Delta J_0) + 2\beta\mathcal{H}^2 + (b + d - 4\beta)(\mathcal{A}^2 + \mathcal{B}^2) \\ &\quad - \alpha \sin \phi \left(\frac{\mathcal{H}^2\mathcal{B}}{\mathcal{A}} + \frac{\mathcal{H}^2\mathcal{A}}{\mathcal{B}} + 4\mathcal{A}\mathcal{B} \right) + \beta \cos \phi \left(\frac{\mathcal{H}^2\mathcal{B}}{\mathcal{A}} + \frac{\mathcal{H}^2\mathcal{A}}{\mathcal{B}} - 4\mathcal{A}\mathcal{B} \right), \end{aligned}$$

where $\phi = \psi_A - \psi_B - 2\theta$. One steady state solution of these equations takes the form $(\mathcal{H}, \mathcal{A}, \mathcal{B}, \phi) = (\hat{\mathcal{H}}, \hat{\mathcal{A}}, -\hat{\mathcal{A}}, \hat{\phi})$, where

$$(62) \quad \hat{\mathcal{H}}^2 = \frac{-\mu\Delta J_0(a + c) - \mu\Delta J_1(-4\alpha + 2(\alpha \cos \hat{\phi} - \beta \sin \hat{\phi}))}{\alpha(a + c) - [4\alpha - 2(\alpha \cos \hat{\phi} - \beta \sin \hat{\phi})][2\alpha - (\alpha \cos \hat{\phi} - \beta \sin \hat{\phi})]},$$

$$(63) \quad \hat{\mathcal{A}}^2 = \frac{-\mu\Delta J_0(-2\alpha + (\alpha \cos \hat{\phi} - \beta \sin \hat{\phi})) - \mu\Delta J_1\alpha}{\alpha(a + c) - [4\alpha - 2(\alpha \cos \hat{\phi} - \beta \sin \hat{\phi})][2\alpha - (\alpha \cos \hat{\phi} - \beta \sin \hat{\phi})]},$$

and $\hat{\phi}$ is found by plugging Eqs.62 and 63 into Eq.61 and setting the left hand side equal to zero. We do not study the stability of the mixed-mode state here.

A.2.2. *Double zero eigenvalue: Turing, Hopf.* $\vartheta(\epsilon)$: The solutions to the linear equation are time periodic oscillations and spatially periodic functions

$$r_1 = H(T) + e^{i\omega t} + A(T)e^{ikx} + c.c.$$

$\vartheta(\epsilon^2)$: The nonlinear forcing and resulting second order solution are

$$\begin{aligned}
 N_2 &= \Phi'' J_0^2 (H^2 e^{2i\omega(t-D)} + c.c. + 2|H|^2)/2 + \Phi'' J_k^2 (A^2 e^{2ikx} + c.c. + 2|A|^2)/2 \\
 &\quad \Phi'' J_0 J_k H A e^{ix+i\omega t} + \Phi'' J_0 J_k A \bar{H} e^{-i\omega t+ix} + c.c., \\
 r_2 &= r_{2H} e^{2i\omega t} + r_{2A} e^{2ikx} + r_{AH} e^{i\omega t+ix} + r_{A\bar{H}} e^{-i\omega t+ix} + c.c. + r_{20}, \\
 r_{AH} &= \frac{\Phi'' J_0 J_k}{i\omega + 1 - \Phi' J_k e^{-i\omega D}} e^{-i\omega D} AH, \\
 r_{A\bar{H}} &= \frac{\Phi'' J_0 J_k}{-i\omega + 1 - \Phi' J_k e^{i\omega D}} e^{i\omega D} A\bar{H}, \\
 r_{20} &= \frac{\Phi'' (J_0^2 |H|^2 + J_k^2 |A|^2)}{1 - J_0 \Phi'}.
 \end{aligned}$$

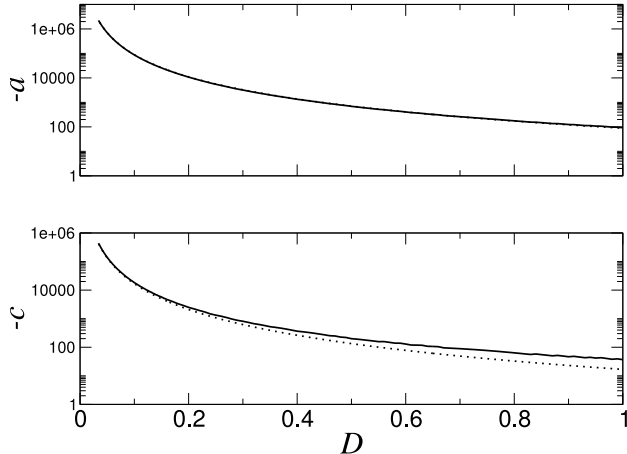


FIGURE 15. Top: The real part of the cubic coefficient at the codimension-2 point. The solid line is the full expression, Eq.55 and the dotted line is the asymptotic result in the $D \rightarrow 0$ limit, Eq.57. Bottom: The real part of the cross-coupling coefficient at the codimension-2 point. The solid line is the full expression, Eq.56 and the dotted line is the asymptotic results in the $D \rightarrow 0$ limit, Eq.58.

$\vartheta(\epsilon^3)$: The nonlinear forcing at cubic order is

$$\begin{aligned} N_3 = & \left(\Phi''(J_0^2 H r_{20} + J_0^2 \bar{H} r_{2H} + J_k^2 A \bar{r}_{A\bar{H}} + J_k^2 \bar{A} r_{AH}) + \Phi''' J_0^2 J_k |H|^2 A + \Phi''' J_k^3 |A|^2 A / 2 \right) e^{i\omega t} \\ & + \left(\Phi''(J_0 J_k H r_{A\bar{H}} + J_0 J_k \bar{H} r_{AH} + J_0 J_k A r_{20} + J_k J_{2k} \bar{A} r_{2A}) + \Phi''' J_0^2 J_1 |H|^2 A \right. \\ & \quad \left. + \Phi''' J_k^3 |A|^2 A / 2 \right) e^{ix}. \end{aligned}$$

Eliminating terms with dependencies $e^{i\omega t}$, e^{ix} yields the two coupled amplitude equations, Eqs.39a-39b,

$$\begin{aligned} \partial_T H &= (\mu + i\Omega) \Delta J_0 H + (\alpha + i\beta) |H|^2 H + (\kappa + i\Lambda) |A|^2 H, \\ \partial_T A &= \bar{\eta} \Delta J_k A + \Gamma |A|^2 A + \sigma |H|^2 A, \end{aligned}$$

where $\mu + i\Omega$, $\alpha + i\beta$, $\bar{\eta}$ and Γ are given by Eqs.51, 52, 18a and 18b respectively, and

$$\begin{aligned} (64) \quad \kappa + i\Lambda &= \frac{e^{-i\omega D}}{1 + D\Phi' \bar{J}_0 e^{-i\omega D}} \left(\frac{\bar{J}_0^2 \bar{J}_k^2}{1 - \Phi' \bar{J}_0} + 2 \frac{\bar{J}_1^3 \bar{J}_0 (\Phi'')^2 e^{-i\omega D}}{i\omega + 1 - \Phi' \bar{J}_1 e^{-i\omega D}} + \Phi''' \bar{J}_0 \bar{J}_1^2 \right), \\ \sigma &= \frac{1}{1 + D\Phi' \bar{J}_1} \left(\bar{J}_0^2 \bar{J}_1^2 (\Phi'')^2 \left(\frac{e^{i\omega D}}{-i\omega + 1 - \Phi' \bar{J}_1 e^{i\omega D}} + \frac{e^{-i\omega D}}{i\omega + 1 - \Phi' \bar{J}_1 e^{-i\omega D}} \right) \right. \\ (65) \quad & \quad \left. + \frac{\bar{J}_0^3 \bar{J}_1 (\Phi'')^2}{1 - \Phi' \bar{J}_0} + \Phi''' \bar{J}_0^2 \bar{J}_1 \right). \end{aligned}$$

In the small delay limit ($D \rightarrow 0$) we can use the asymptotic values Eqs.12 to obtain, to leading order,

$$\begin{aligned} \kappa + i\Lambda &= -\frac{\pi}{2D(\Phi')^3} \frac{(\pi/2 + i)}{(1 + \pi^2/4)} \left(\frac{(\Phi'')^2}{\Phi'} - \Phi''' \right) + \vartheta(1), \\ \eta &= \Phi' + \vartheta(D), \\ \Gamma &= \frac{1}{(\Phi')^3} \left(-\frac{(\Phi'')^2}{\Phi'} + \frac{\Phi'''}{2} + \frac{J_{2k}(\Phi'')}{2(1 - J_{2k}\Phi')} \right) + \vartheta(D), \\ \sigma &= -\frac{\pi^2}{4D^2(\Phi')^3} \left(\frac{(\Phi'')^2}{\Phi'} - \Phi''' \right) + \vartheta(1/D), \end{aligned}$$

and $\mu + i\Omega$ and $\alpha + i\beta$ are given by Eqs.20a and 20b respectively.

REFERENCES

- [Roxin et al.(2005)] A. Roxin, N. Brunel, and D. Hansel, Phys. Rev. Lett. **94**, 238103 (2005).
- [Roxin et al.(2006)] A. Roxin, N. Brunel, and D. Hansel, Prog. Theor. Phys. **161**, 68 (2006).
- [Amit and Brunel(1997)] D. J. Amit and N. Brunel, Cerebral Cortex **7**, 237 (1997).
- [Brunel and Hakim(1999)] N. Brunel and V. Hakim, Neural Comp. **11**, 1621 (1999).
- [Brunel(2000)] N. Brunel, J. Comput. Neurosci. **8**, 183 (2000).
- [Wilson and Cowan(1972)] H. R. Wilson and J. D. Cowan, Biophys. J. **12**, 1 (1972).
- [Ermentrout(1994)] G. B. Ermentrout, Neural Computation **6**, 679 (1994).
- [Shriki et al.(2003)] O. Shriki, D. Hansel, and H. Sompolinsky, Neural Comput. **15**, in press (2003).
- [Holmgren et al.(2003)] C. Holmgren, T. Harkany, B. Svennenfors, and Y. Zilberman, J. Physiol. **551**, 139 (2003).
- [Ben-Yishai et al.(1995)] R. Ben-Yishai, R. Lev Bar-Or, and H. Sompolinsky, Proc. Natl. Acad. Sci. USA **92**, 3844 (1995).
- [Hansel and Sompolinsky(1998)] D. Hansel and H. Sompolinsky, in *Methods in Neuronal Modeling*, edited by C. Koch and I. Segev (MIT press, Cambridge, MA, 1998), 2nd ed.
- [Coombes et al.(2003)] S. Coombes, G. J. Lord, and M. R. Owen, Physica D **178**, 219 (2003).
- [Atay and Hutt(2005)] F. M. Atay and A. Hutt, SIAM J. Appl. Math. **65**, 644 (2005).
- [Venkov et al.(2007)] N. A. Venkov, S. Coombes, and P. C. Matthews, Physica D **232**, 1 (2007).
- [Pinto and Ermentrout(2001)] D. J. Pinto and G. B. Ermentrout, SIAM J. Appl. Math. **62**, 226 (2001).
- [Hutt et al.(2003)] A. Hutt, M. Bestehorn, and T. Wennekers, Network: Comput. Neural Syst. **14**, 351 (2003).
- [Hutt(2004)] A. Hutt, Phys. Rev. E **70**, 052902 (2004).
- [Laing and Coombes(2005)] C. R. Laing and S. Coombes, Network **17**, 151 (2005).
- [Hutt and Atay(2006)] A. Hutt and F. M. Atay, Phys. Rev. E **73**, 021906 (2006).
- [Coombes et al.(2007)] S. Coombes, N. A. Venkov, L. Shiau, I. Bojak, D. T. J. Liley, and C. R. Laing, Phys. Rev. E **76**, 051901 (2007).
- [Cross and Hohenberg(1993)] M. C. Cross and P. C. Hohenberg, Rev. Mod. Phys. **65**, 851 (1993).
- [Hutt et al.(2008)] A. Hutt, C. Sutherland, and A. Longtin, Phys. Rev. E **78**, 021911 (2008).
- [Roberts and Robinson(2008)] J. A. Roberts and P. A. Robinson, Phys. Rev. E **78**, 051901 (2008).
- [Coombes and Laing(2009)] S. Coombes and C. Laing, Philos. Trans. R. Soc. A **367**, 1117 (2009).
- [Thomson and Lamy(2007)] A. M. Thomson and C. Lamy, Frontiers in Neuroscience **1**, 19 (2007).
- [Kandel et al.(1991)] E. Kandel, J. H. Schwartz, and T. M. Jessell, *Principles of neural science* (McGraw-Hill, 1991).
- [Girard et al.(2001)] P. Girard, J. M. Hupé, and J. Bullier, J. Neurophysiol. **85**, 1328 (2001).

- [Ermentrout and Cowan(1980)] G. B. Ermentrout and J. D. Cowan, SIAM J. on Appl. Math. **38**, 1 (1980).
- [Miller and Troyer(2002)] E. K. Miller and T. W. Troyer, J. Neurophysiol. **87**, 653 (2002).
- [Hansel and van Vreeswijk(2002)] D. Hansel and C. van Vreeswijk, J. Neurosci. **22**, 5118 (2002).
- [Hellwig(2000)] B. Hellwig, Biol. Cyber. **82**, 111 (2000).
- [Wang and Buzsáki(1996)] X.-J. Wang and G. Buzsáki, J. Neurosci. **16**, 6402 (1996).
- [Holmes(1995)] M. H. Holmes, *Introduction to Perturbation Methods* (Springer, New York, 1995).

ALEX ROXIN
CENTER FOR THEORETICAL NEUROSCIENCE
COLUMBIA UNIVERSITY
NEW YORK
NEW YORK, USA

COMPUTATIONAL NEUROSCIENCE GROUP
DEPARTMENT OF INFORMATION AND COMMUNICATION TECHNOLOGIES
UNIVERSITAT POMPEU FABRA
08003 BARCELONA, SPAIN

ERNEST MONTBRIÓ
CENTER FOR NEURAL SCIENCE
NEW YORK UNIVERSITY
NEW YORK
10012 NEW YORK, USA

COMPUTATIONAL NEUROSCIENCE
DEPARTMENT OF INFORMATION AND COMMUNICATION TECHNOLOGIES
UNIVERSITAT POMPEU FABRA, BARCELONA, SPAIN

CENTRE DE RECERCA MATEMTICA (CRM)
BELLATERRA, BARCELONA, SPAIN